Summary Report: Glass-Ceramic Waste Forms for Combined Fission Products

Fuel Cycle Research & Development

Prepared for
U.S. Department of Energy
Waste Form Campaign
J.V. Crum, B.J. Riley, and L.R. Turo
Pacific Northwest National Laboratory
M. Tang and A. Kossoy
Los Alamos National Laboratory

September 23, 2011

FCRD-WAST-2011-000358
PNNL-20749

Fuel Cycle Research and Development
Document Cover Sheet

Name/Title of Deliverable/Milestone	Summary Report: Glass-Ceramic Waste Forms for Combined Fission Products / Summary Report for FY 2011 Glass Ceramic Development / M31SW090404
Work Package Title and Number	Glass Ceramic FTPN11SW0904
Work Package WBS Number	1.02.03.09 Alternative Waste Forms
Responsible Work Package Manager	Jarrod Crum (Name/Signature)

Date Submitted 9/23/2011

Quality Rigor Level for Deliverable/Milestone ☒ Rigor Level 3 ☐ Rigor Level 2 ☐ Nuclear Data

This deliverable was prepared in accordance with Pacific Northwest National Laboratory
(Participant's (National Laboratory or Subcontractor) Name)

QA program which meets the requirements of

☒ DOE Order 414.1 ☐ Nuclear Data Requirements

This Deliverable was subjected to:

☒ Independent Technical Review ☐ Peer Review

Independent Technical Review (ITR)	Peer Review (PR)	Nuclear Data Validation (NDV)
Review Documentation Provided	**Review Documentation Provided**	**Review Documentation Provided**
☐ **Signed ITR Report or,**	☐ **Signed PR Report or,**	☐ **Signed Validation Documentation or,**
☐ **Signed ITR Concurrence Sheet or,**	☐ **Signed PR Concurrence Sheet or,**	☐ **Signed Validation Concurrence or,**
☐ **Signature of ITR Reviewer(s) below**	☐ **Signature of PR Reviewer(s) below**	☐ **Signature of Validation Reviewer(s) below,**

Name and Signature of Peer Reviewers(s)/Independent Technical Reviewer(s) (NOTE: Electronic signatures or other proof of approval (e-mails, other electronic verification) may be provided in lieu of signatures on this form)

John S McCoy - Johns, McCoy 9-23-11

SUMMARY

Glass-ceramic waste form development began in fiscal year (FY) 2010 by examining two combined waste stream options: Option 1) alkali/alkaline earth (CS) + lanthanide (Ln); and Option 2) + transition metal (TM) fission-product waste streams generated by the uranium extraction separations process. Glass ceramics were successfully developed for both options; however, Option 2 was selected over Option 1 at the conclusion of 2010, because Option 2 immobilized all three waste streams with only a minimal decrease in waste loading.

During the first year, a series of three glass ceramics (Option 2) were fabricated that varied waste loading ([WL] 42, 45, and 50 mass%) at fixed molar ratios of CaO/MoO_3 and B_2O_3/alkali both at 1.75. These glass ceramics were slow-cooled and characterized in terms of phase assemblage and preliminary irradiation stability.

This FY, further characterization was performed on the FY 2010 Option 2 glass ceramics in terms of static leach testing, phase analysis by transmission electron microscopy, and irradiation stability (electron and ion). In addition, a new series of glass ceramics were developed for Option 2 that varied the additives: Al_2O_3 (0-6 mass%), molar ratio of CaO/MoO_3 and B_2O_3/alkali (1.75-2.25), and waste loading (50, 55, and 60 mass%). Phase-pure powellite and oxyapatite were then synthesized for irradiation studies.

Results from this FY study showed compositional flexibility, chemical stability, and radiation stability in the current glass-ceramic system. First, the phase assemblages and microstructure of all of the FY 2010 and FY 2011 glass ceramics are very similar when subjected to the slow-cool heat treatment. The phases identified in these glass ceramics were oxyapatite, powellite, cerianite, and Ln-borosilicate. This shows that variations in waste loading or additives can be accommodated without drastically changing the phase assemblage of the waste form, thus making the processing and performance characteristics of the waste form more predictable/flexible. However, in the future, the glass phase still needs to be accurately characterized to determine the effects of waste loading and additives on the glass structure. Initial investigations show a borosilicate glass phase rich in silica.

Second, the normalized concentrations of elements leached from the waste form during static leach testing were all below 0.6 g/L after 28 days at 90°C, by the product consistency test method B. These normalized concentrations are comparable to chemically durable waste glasses such as the low-activity reference material glass (Ebert and Zyryanov 2000). The release rates for the crystalline phases (oxyapatite and powellite) appear to be lower (more durable) than the glass phase based on the relatively low release rates of Mo, Ca, and Ln found in the crystalline phases compared to Na and B that are mainly observed in the glass phase. However, further static leach testing on individual crystalline phases is needed to confirm this statement.

Third, ion irradiation and in situ transmission electron microscopy observations indicate these crystalline phases (such as oxyapatite, Ln-borosilicate, and powellite) in silicate based glass-ceramic waste forms exhibit stability to 1000 years at anticipated doses (2×10^{10}-2×10^{11} Gy). This is adequate for the short-lived isotopes in the waste, which lead to a maximum cumulative dose of ~7×10^{9} Gy, reached after ~100 years, beyond which the dose contributions are negligible. The cumulate dose calculations are based on a glass ceramic at WL = 50 mass%, where the fuel has a burn-up of 51 GWd/MTIHM (or gigawatt-day per metric ton of initial heavy metal), immobilized after a 5-year decay from reactor discharge.

Future work on the glass-ceramic waste form will focus on examining processing properties to support a melter test. In addition, a new series of glass ceramics will vary key waste components (MoO_3, ZrO_2, and Ln_2O_3) and additives (B_2O_3, CaO, Al_2O_3, and SiO_2) to examine the effects of individual waste/additive components on waste form properties.

CONTENTS

FIGURES

TABLES

ACRONYMS, ABBREVIATIONS, AND DEFINITIONS

AFCI	Advanced Fuel Cycle Initiative
BF	bright field
CS	alkaline/alkaline earth fission products
EDS	energy dispersive spectroscopy
EML	Electron Microscope Laboratory
EXAFS	X-ray absorption fine structure
FY	fiscal year
HLW	high-level waste
LANL	Los Alamos National Laboratory
Ln	lanthanide fission products or lanthanides
LRM	low-activity reference material
MTIHM	metric tons of initial heavy metal
Option 1	CS + Ln combined waste stream
Option 2	CS + Ln + TM combined waste stream
PCT	product consistency test
PDF-2	Powder Diffraction File
PNNL	Pacific Northwest National Laboratory
RT	room temperature
RO	alkaline earth oxide
R_2O	alkali oxide
SAED	select area electron diffraction
SEM	scanning electron microscope(y)
SRM	standard reference material
STEM	scanning transmission electron microscopy
T_d	dilatometric softening point
TEM	transmission electron microscopy
TEOS	tetraethyl orthosilicate
T_g	glass transition temperature
T_L	liquidus temperature
T_M	glass melting temperature
TM	transition metal fission products
UREX$^+$	uranium extraction process
XANES	X-ray Absorption Near Edge Structure

XPS	X-ray photoelectron spectroscopy
XRD	X-ray diffraction

WASTE FORMS CAMPAIGN/FCR&D PROGRAM

1. INTRODUCTION

Development of a glass-ceramic waste form began in fiscal year (FY) 2010 to examine two different combined waste stream options: 1) alkali/alkaline earth (CS) + lanthanide (Ln), and 2) CS + Ln + transition metal (TM) fission-product waste streams generated by the uranium extraction ($UREX^+$) separations process, with the results summarized (Crum et al. 2010). Results showed glass ceramic has the potential to at least double waste loading of the combined CS + Ln + TM waste streams (Option 2), compared to the current baseline, borosilicate glass (Crum et al. 2010; Gombert et al. 2009; Crum et al. 2009; Ryan et al. 2009). Option 2 was preferred over Option 1 because it would not require an additional treatment process to immobilize the TM fission products while achieving similar waste loading levels as those achieved for the Option 1 glass-ceramics (Crum et al. 2010). Thus, Option 1 glass-ceramic development was put on hold at the end of FY 2010.

Glass-ceramic development work for FY 2011 focused on further characterization of the previous year's Option 2 glass-ceramic compositions. This year's work focused on further characterization of pre-existing glass ceramics, development of new glass ceramics, and synthesis of single phases.

The FY 2010 glass-ceramic compositions were subjected to static leach testing by the product consistency test (PCT) method B for durations of 3 and 28 days ("Standard Test Methods for Determining Chemical Durability of Nuclear, Hazardous, and Mixed Waste Glasses and Multiphase Glass Ceramics: The Product Consistency Test (PCT)" 2002). Scanning transmission electron microscopy (STEM) and transmission electron microscopy (TEM) were performed on a slow-cooled glass to provide finer detail on the microstructure and chemistry compared to the scanning electron microscope (SEM) work previously done. Additionally, electron, proton, and light ion irradiation testing was performed on Option 2 compositions from FY 2010.

A new series of glass-ceramic compositions were formulated to vary the concentrations of additives (B_2O_3, Al_2O_3, and CaO) and waste loading to determine how stable the crystalline phases (oxyapatite, Ln-borosilicate, powellite, and cerianite) are to changes in chemistry. Samples of each were subjected to isothermal and slow-cool heat treatments, which were analyzed with X-ray diffraction (XRD) and SEM, and compared to FY 2010 compositions.

We then synthesized phase pure powellite and oxyapatite to gain a better understanding of irradiation damage and avoid any interactions caused by the complex multiphase glass ceramics. Powellite was synthesized from oxides by crystallizing from a melt. The liquidus temperature of oxyapatite (T_L ~ 1980°C) is above the maximum operating temperature of the furnaces available so the batch was mixed by the sol-gel method followed by traditional cold press and sinter (Celerier et al. 2006; Bondar 1982).

2. METHODS

2.1 Glass Ceramic Fabrication

Glass ceramics were batched from oxides, carbonates, boric acid, and Ru-nitrate in solution (*Glass Batching and Melting*). Ruthenium oxide was added to Option 1 glass ceramics only in the form of Ru-nitrate dissolved in water to ensure intimate mixing with the dry chemicals during the batching process. Once the Ru-nitrate solution dried onto the batch materials, the batch was mixed in an agate milling chamber for 4 minutes. The glasses were melted between 1200°C and 1350°C for 1 hour and cast onto a steel plate. The quenched glass was ground in a tungsten carbide milling chamber for 4 minutes to rehomogenize chemically for any heavy elemental segregation during the first melt and then remelted for 1 hour and quenched on a stainless-steel plate.

2.1.1 Isothermal Heat Treatment

Quenched glass samples were loaded into platinum crucibles, with tight-fitting lids, and heat treated at various temperatures between 750–1250°C for 4 hours, followed by a rapid air quenched, to determine the crystalline phases formed and their morphologies.

2.1.2 Controlled Cool Heat Treatment

Glass ceramics were formed by a controlled cooling schedule, as depicted in Figure 1, that was selected to follow the canister centerline cooling curve determined for a 2" diameter canister (André 2004; Petkus 2003). Samples were loaded into platinum boats with tight-fitting lids and placed in a furnace at the melting temperature. The furnace was then cooled to room temperature according to the calculated slow-cooling profile for a 0.61 m (2-ft) diameter canister.

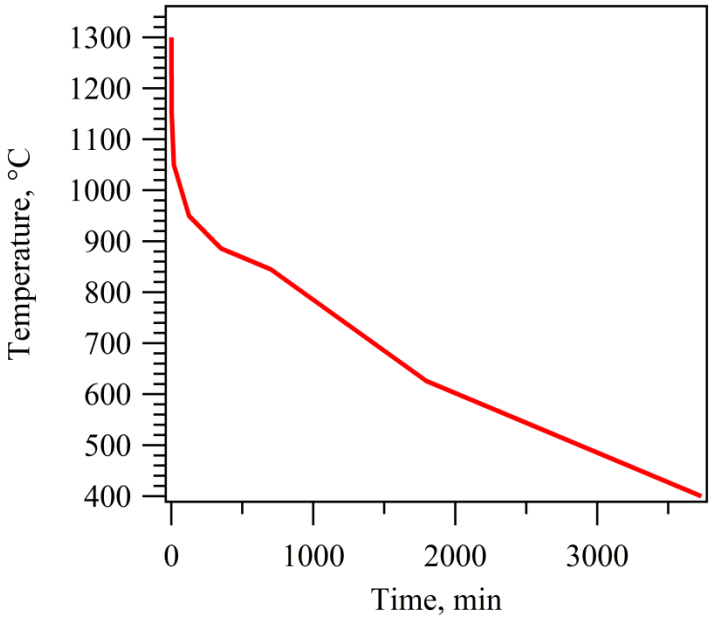

Figure 1. Slow-cool heat treatment temperature profile.

2.1.3 Powellite Synthesis Method

To make single-phase powellite, a 20 g batch (oxide basis), using $CaCO_3$ and MoO_3 precursors, was weighed to the nearest 0.01 g and milled in a high-energy shaker mill for 4 minutes. The batch was transferred to a platinum crucible, with a tight-fitting lid, and placed into a furnace at 1500°C for 30 minutes. The batch was then cooled at 1°C/min to 1400°C and held 4 hours. The batch was then cooled at 1°C/min down to room temperature.

2.1.4 Oxyapatite Synthesis Method

Two methods were examined to synthesize phase pure oxyapatite.

1. The traditional ceramic preparation method was followed. A 20 g batch (oxide basis) using $CaCO_3$, Nd_2O_3, and SiO_2 precursors, was milled overnight on a ball mill with zirconium media to reduce particle size and provide mixing. The batch was dried at 105°C and calcined at 1000°C for 1 hour to remove carbonate and then cooled in a desiccator. Powders were pressed into ~ 19-mm diameter pellets of ~3 g using an isostatic press up to ~3×10^8 Pa. The pellets were fired by ramp heating at 3°C/min to 1250°C and held for 24 hours, followed by cooling at 3°C/min down to room temperature. This method did not result in a phase pure sample according to XRD results and showed some

unreacted Nd_2O_3. This method was abandoned because we came to the conclusion that inadequate mixing was the problem.

2. Célérier et al., successfully produced a oxyapatite ($La_{9.33}Si_6O_{26}$) by a sol-gel process, that we closely followed to prepare a batch of oxyapatite (Celerier et al. 2006). However chemistry was changed to produce an oxyapatite ($Ca_2Nd_8Si_6O_{26}$) more representative of the oxyapatite found in the glass ceramics. The batch was prepared by combining 3.53 g $Ca(NO_3)_2 \cdot 4H_2O$, 26.20 g $Nd(NO_3)_3 \cdot 6H_2O$, 20 mL of ethanol, and 20 mL of glacial acetic acid in a Pyrex beaker. The beaker was maintained at room temperature and continuously stirred with a serpentine-shaped platinum stirring rod. After the solids dissolved into solution, 10 mL of tetraethyl orthosilicate (TEOS) was added to the solution and stirred for 1 hour. The solution thickened but remained a clear bluish-purple liquid. The liquid was then dried overnight at 80°C to remove water/ethanol, creating a clear bluish-purple solid. The batch was calcined at 1000°C to convert to oxides. Pellets were pressed and fired following the same steps performed for the first method. The sample was shown to be phase-pure oxyapatite by XRD.

2.2 Characterization

2.2.1 Scanning Electron Microscope/Energy Dispersive Spectroscopy

Polished cross-sections were sputter coated with palladium and then loaded into the SEM to examine the morphology and elemental chemistry of the crystalline phases. The SEM used was a JEOL 5900 (JEOL, Ltd., Tokyo, Japan) with a tungsten wire filament. It is equipped with an energy dispersive spectroscopy (EDS) system for elemental analysis. The EDS detector is an EDAX Si-drifted detector (AMETEK, Berwyn, PA).

2.2.2 X-Ray Diffraction

Samples were spiked with a known concentration of an internal standard, SRM 674b and powdered in a tungsten carbide milling chamber ("X-ray Power Diffraction Intensity Set for Quantitative Analysis by X-Ray Diffraction" 2007). Samples were pressed into a standard 25-mm-diameter powder mount. The powder mount was then loaded into a Bruker D8 Advance diffractometer (Bruker AXS Inc., Madison, WI). The D8 has a Cu X-ray target, a goniometer radius of 250 mm, a 0.3° fixed divergence slit, and a LynxEye position sensitive detector with an angular range of 3°. Scan parameters are as follows: range 5 to 70° 2θ, step size 0.015° 2θ, and a hold time of 0.3 s/step. Crystalline phases were identified with Jade 6.0 software equipped with both the International Center of Crystallographic Data PDF2 release 1999 and the International Center of Structure Data release 2004. Whole pattern fitting was done using TOPAS 4.2 software to determine the quantitative fractions of the crystalline phases. Fitting was done using the fundamental parameters approach (Cheary et al. 2004).

2.2.3 Transmission Electron Microscopy and Scanning Transmission Electron Microscopy

Samples were prepared in plan-view geometry for TEM and STEM examination. Final thinning to electron transparency was accomplished using 4-5 keV Ar^+ ion milling. The ion milling caused some damage in the form of holes in the GC-5.86-SC TEM sample. Microstructure and elemental chemistry of the crystalline phases were examined using two different TEMs.

1. FEI Tecnai F30 (FEI Company, Hillsboro, OR) TEM operating at 300 kV in the Electron Microscope Laboratory (EML) at Los Alamos National Laboratory (LANL).

2. At Pacific Northwest National Laboratory (PNNL), a JEOL 2010F field emission TEM at an accelerating voltage of 200 kV using bright field (BF) and diffraction techniques.

3. An elemental dot map was collected by Carl Zeiss Nano Technology Systems North America in STEM mode on a Ziess Ultra^{+} SEM.

2.2.4 Ion Beam Irradiation

Preliminary evaluations of the radiation damage tolerance of the glass ceramic waste forms were performed at LANL. Protons (H^{+}), helium (He^{+}), and electrons (e^{-}) were used to simulate the self-radiation damage that occurs in a material incorporating nuclides that are undergoing radioactive decay. Most of the self-irradiation in a waste form incorporating fission products is due to beta (β) particle and gamma (γ) emissions. These emissions cause radiation damage primarily via radiolytic processes—both β and γ particles induce substantial electronic excitations in a target material. However, if β and γ particles are only partially attenuated by the surrounding waste form, a significant fraction of the energy may escape. Proton, alpha, and electron particles provide a useful means to examine radiolysis effects because they deposit nearly all of their energy in solids via electronic loss processes (electronic-to-nuclear stopping power ratio of nearly 2000 for 3 MeV H^{+} in SiO_2). As such, these tests provide an upper bound for the β and γ emissions in the waste form.

In these experiments, the authors of this report irradiated samples in the Ion Beam Materials Laboratory at LANL, with 3 MeV H^{+} and 5 MeV He^{+} ions generated in a 3.2 MV tandem ion accelerator with the samples at room temperature (25°C) and 230°C. The elevated temperature served to simulate decay heats representative of different radionuclide loadings of a waste form. For the electron beam irradiation study, a TEM specimen was prepared in plan-view geometry. This plan-view sample was examined at room temperature in an FEI Tecnai F30 electron microscope operating at 300 kV. Electron irradiation experiments were conducted by focusing the electron beam onto small regions of electron transparent material (a typical irradiated region was ~100 nm diameter).

2.2.5 Nano-indentation

Preliminary evaluations of the mechanical property of the glass ceramic waste forms were performed at LANL using nano-indentation techniques. The nano-indentation test on GC-4, from FY 2010 (Crum et al. 2010), samples before and after ion irradiation was performed on a MTS Nano XP Nanoindenter, with a Berkovich tip (three-sided pyramid, with a 1:7 depth to width ratio). The indents will be approximately 300 nm deep, so they should be about 2.1 micron wide. Young's modulus and hardness of certain crystalline phases in GC-4 samples were measured.

3. GLASS FORMULATION

During FY 2010, the molar ratios of B_2O_3/alkali and CaO/MoO_3 were fixed at 1.75 (Caurant et al. 2007) to force a Ca-rich molybdate with the powellite/scheelite structure, while waste loading was varied at 42, 45, and 50 mass%. The glasses were formulated to melt at ~ 1250–1300°C to avoid volatility of alkali (mainly Cs_2O) and MoO_3. These glass ceramics successfully formed Ca-rich powellite that also contained some lanthanides.

For FY 2011, a series of new glass-ceramic compositions (Table 1), were formulated to vary the molar ratios of B_2O_3/alkali and CaO/MoO_3 (1.75–2.25), Al_2O_3 (0–6 mass %) and waste loading (50–55 mass%) to evaluate how sensitive powellite, oxyapatite, and Ln-borosilicate are to moderate changes in chemistry. There will likely be changes in crystalline phase concentrations related to changes in additives and waste loading. However, the crystalline phase types should ideally remain unchanged. The glasses were again designed to melt at ~ 1250–1300°C.

Table 1. Glass-ceramic compositions, in mass % (FY 2010 and FY 2011) given with design criteria.

	FY 2010				FY 2011							
Components	GC-5.86	GC-6.25	GC-6.94		GC-6.94-2	GC-6.94-3	GC-6.94-4	GC-6.94-5	GC-7.6-1	GC -7.6-2	GC -8.3-1	GC -8.3-2
Al_2O_3	6.0	5.0	5.0		3.0	5.0	5.0	5.0	4.0	4.5	3.1	0.0
B_2O_3	9.5	9.4	8.4		8.3	8.5	7.8	9.3	6.6	6.3	5.2	6.7
CaO	4.0	4.3	4.7		4.7	6.1	6.1	4.7	5.2	6.7	5.7	7.3
Na_2O	3.7	3.5	2.9		2.8	2.0	2.6	2.3	1.8	1.0	1.0	1.0
SiO_2	34.8	32.8	29.0		31.1	28.5	28.5	28.7	27.4	26.5	25.0	25.0
MoO_3	5.8	6.2	6.9		6.9	6.9	6.9	6.9	7.6	7.6	8.3	8.3
RO waste	4.8	5.1	5.7		5.7	5.7	5.7	5.7	6.2	6.2	6.8	6.8
R_2O waste	4.9	5.3	5.9		5.9	5.9	5.9	5.9	6.4	6.4	7.0	7.0
Ln_2O_3	20.0	21.4	23.8		23.8	23.8	23.8	23.8	26.2	26.2	28.6	28.6
Other	6.5	6.9	7.7		7.7	7.7	7.7	7.7	8.5	8.5	9.3	9.3
Design Criteria												
Waste loading, mass%	42	45	50		50	50	50	50	55	55	60	60
Al_2O_3, mass%	6	5	5		3	5	5	5	4	4	3	0
CaO/MoO_3, mole basis	1.75	1.75	1.75		1.75	2.25	2.25	1.75	1.75	2.25	1.75	2.25
B_2O_3/Alkali, mole basis	1.75	1.75	1.75		1.75	2.25	1.75	2.25	1.75	2.25	1.75	2.25

RO = SrO and BaO; R_2O = Rb_2O and Cs_2O; alkali = Rb_2O, Cs_2O, and Na_2O; Ln_2O_3 = lanthanides, Others = Ag_2O, Br, CdO, PdO, RhO_2, RuO_2, Sb_2O_3, SeO_2, SnO_2, TeO_2, and ZrO_2.

4. RESULTS

4.1 Characterization Results for FY 2010 Glass Ceramics

4.1.1 Transmission Electron Microscopy and Scanning Transmission Electron Microscopy Phase Analysis GC-5.86-SC

Plan view TEM images and diffraction patterns are show for Ln-borosilicate (Figure 2) and oxyapatite (Figure 3) crystals found in GC-5.86-SC sample. Figure 4 shows the heterogeneous nature of the powellite crystals in GC-5.86-SC sample. In addition, the powellite crystal appears to be lighter colored in the center with a darker outer ring. These TEM results confirm the structures previously determined by XRD. An elemental dot map was collected on GC-5.86-SC by a SEM configured in STEM mode, providing a clear view of the locations of the major elements in the glass ceramic (Figure 5). The glass phase (matrix) is dominated by SiO_2. Calcium and Mo are present in both crystalline phases (round and needle shapes). The lanthanides (only Nd and Ce shown for clarity) are almost entirely confined to the needle-shaped crystals. Based on these results and the prior XRD analysis, the round crystals are assumed to be powellite and the needle-shaped crystals are either Ln-borosilicate or oxyapatite. The light regions in Figure 2 and Figure 3 and black regions seen in the Si map in Figure 5 are holes in the sample caused by ion milling during the TEM sample preparation.

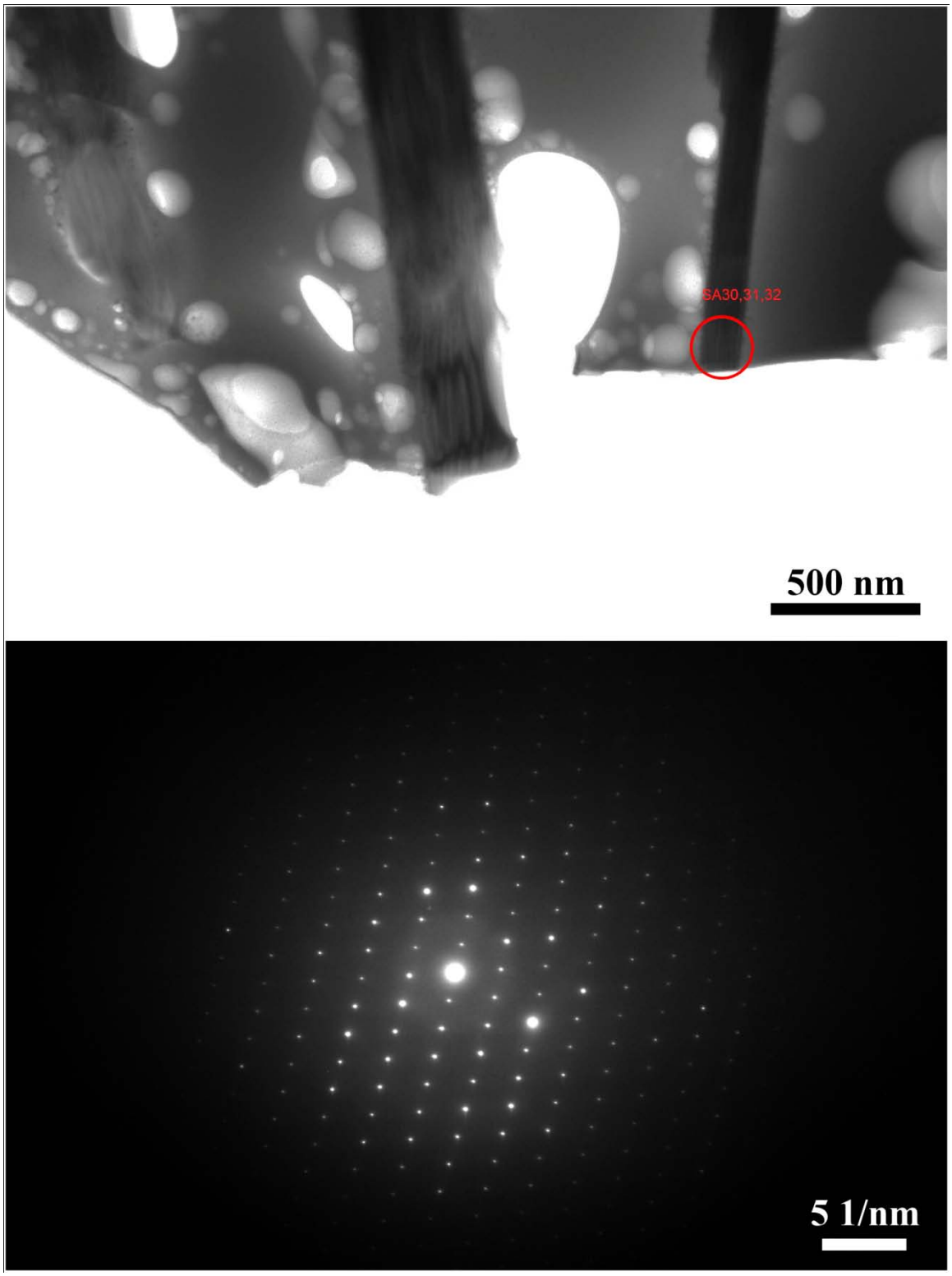

Figure 2. Plan view of Ln-borosilicate crystal shown in top image. Diffraction pattern shown in bottom image, red circle shows diffraction pattern location.

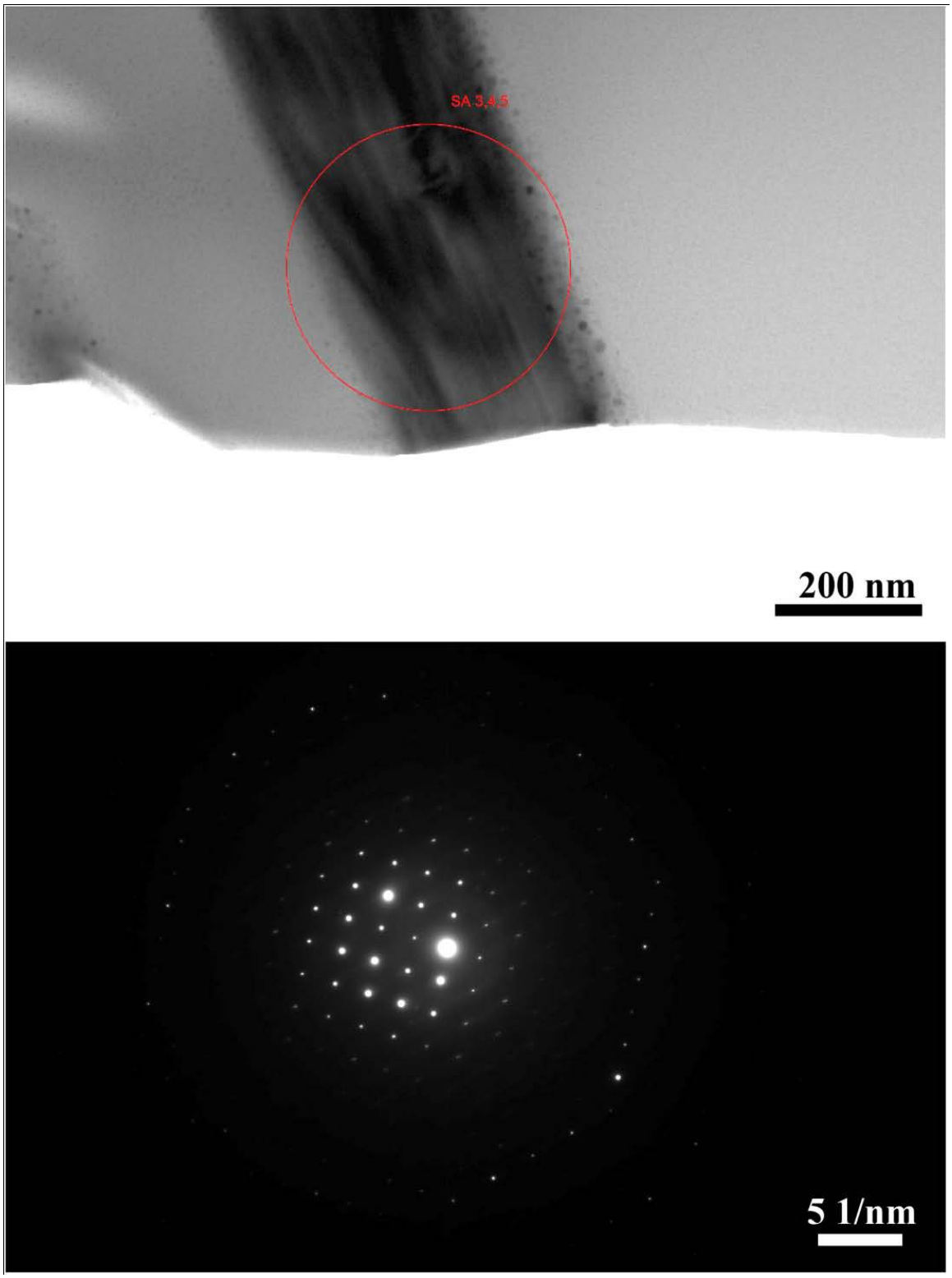

Figure 3. Plan view of Oxyapatite crystal shown in top image. Diffraction pattern shown in bottom image, red circle shows diffraction pattern location.

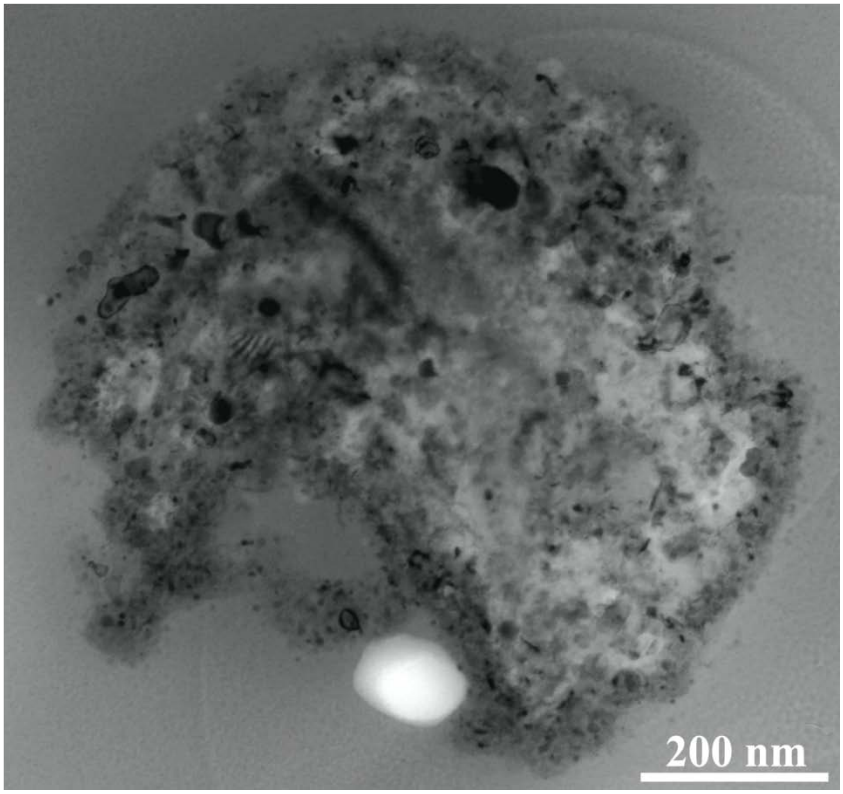

Figure 4. TEM image of powellite crystal with heterogeneous nature.

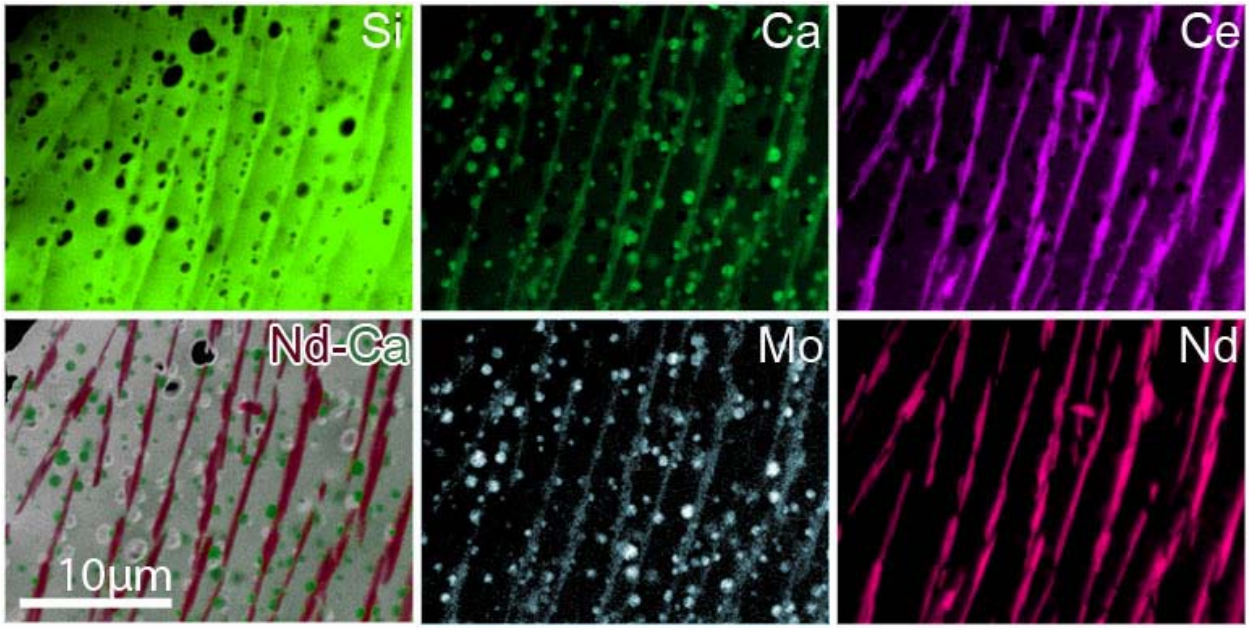

Figure 5. Elemental dot map of GC-5.86-SC sample collected in STEM mode.

4.1.2 Static Leach Results

The static leach testing results collected in duplicate for the GC-5.86-SC, GC-6.25-SC, and GC-6.94-SC are shown (averaged) in Figure 6, as measured by PCT-B at durations of 3 and 28 days as normalized

concentrations (normalized to target composition). The normalized concentrations are consistent with the low-activity reference material (LRM) glass(Ebert and Zyryanov 2000). The highest normalized concentration after the 28-day test is Na at ~0.6 g/L (GC-6.94-SC). The normalized concentrations of Na, Cs, and B tend to increase with time and are believed to be mainly contained in the glass phase. Mo also increased with time for the GC-6.94-SC sample only. For the other two samples, GC-5.86-SC and CG-6.25-SC, the Ca and Mo, which are mainly confined to the powellite phase (based on SEM), have low normalized concentrations in solution that remain almost constant with time. The normalized concentrations for the lanthanides (for clarity only Nd shown) are all very low and flat with respect to time. The lanthanides are for the most part contained in either the Ln-borosilicate or oxyapatite phases.

The glass phase appears to leach faster than the crystalline phases based on the varied release rates of the different elements in the glass-ceramic waste form. GC-6.94-SC has release rates that are approximately double that of the other two glasses for most of the elements analyzed. However, the normalized concentrations are all low showing that these glass ceramics are quite durable, based on these short-term leach tests. Long-term leach testing is the next logical step to evaluate these glass ceramics and determine if a corrosion product could form that may negatively impact the leach rates.

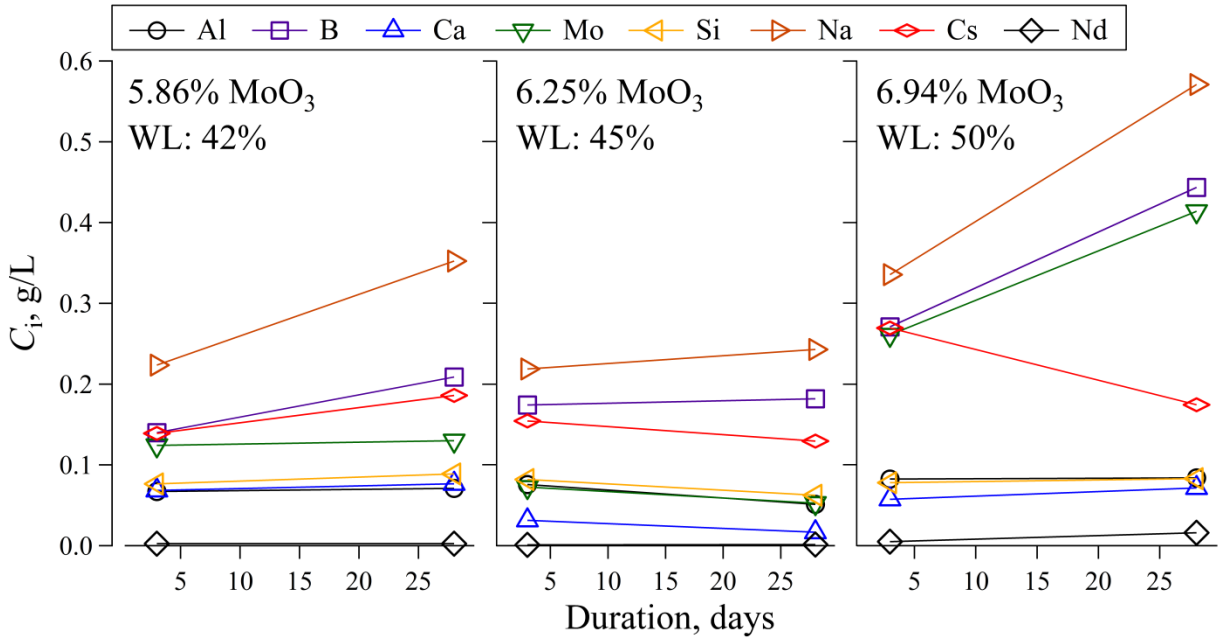

Figure 6. Normalized release as a function of time for GC-5.86-SC, GC-6.25-SC, and GC-6.94-SC as measured according to the PCT-B method.

4.2 Results for Fiscal Year 2011 Glass-Ceramic Compositions

4.2.1 Melt Observations Before Crystal Growth

All of the glass ceramics at a waste loading of 50 mass%, poured at 1300°C from the melting crucible at the end of the second melts. Both GC-7.6-1 and GC-7.6-2 at waste loading of 55 mass%, melted but GC-7.6-2 poured while GC-7.6-1 was highly viscous and remained in the crucible. At the end of the GC-7.6-2 melt, the platinum showed signs of leaks, indicating the melts may have corroded the crucible. To date, the melting of GC-8.3-1 and 2, the highest waste loading (60 mass%), has not been completed. They will be attempted in early FY 2012.

All of the glass-ceramic compositions that were melted appeared a brownish color caused by crystalline phase separation upon quenching from a melt, similar to previous compositions. Figure 7 shows an

example of a glass-ceramic quenched from a melt. The dark regions were in direct contact with the steel quench plate and appear as single-phase glass while the vast majority of the sample was phase-separated (crystalline) causing the brownish color.

The mass before and after melting was recorded to approximate volatility that occurred during melting. The glasses showed mass losses of GC-6.94-2 = 2.8 mass%, GC-6.94-3 = 1.1 mass%, GC-6.94-4 = 3.5 mass%, and GC-6.94-5 = 3.2 mass% after the first melt. These mass losses were corrected for the mass loss expected from decomposition of H_3BO_3 and carbonates. There is some error in these measurements because each glass is poured onto a quench plate and broken into smaller chunks. Thus, a some small amount of the glass can be lost as small pieces of glass. As a result, these values are likely overestimations of the actual mass loss.

Figure 7. As-melted glass ceramic quenched on a steel plate from the melting temperature.

4.2.2 X-Ray Diffraction Analysis of Slow-Cooled Samples

A series of compositions, slow-cooled form T_M, are shown in which the ratio of B_2O_3/alkali, CaO/MoO_3 and Al_2O_3 were varied, while waste loading was fixed at 50 mass% are shown in Figure 8 along with identified crystalline phases. The identified crystalline phases (seen in Figure 8), quantitative mass %, and unit cell parameters determined by whole pattern fitting of slow-cooled glass ceramic specimens are summarized in Table 2.

The effects of one-at-a-time changes to the molar ratio of B_2O_3/alkali, CaO/MoO_3, or the mass% Al_2O_3 on crystallinity, in relation to GC-6.94-1-SC (baseline), are plotted in Figure 9. The ratio of B_2O_3/alkali had no significant effect on the total crystallinity or individual phases. However, increasing Al_2O_3 by 2 mass%, resulted in an increase of 4 mass% of oxyapatite and increasing the molar ratio of $CaO/MoO_3$by 0.5 mass% resulted in both 4.7 mass% increase of oxyapatite and 3.5 mass% increase of powellite. These results show some flexibility to control the amounts of individual phases or total crystallinity without changing crystalline phase types.

Table 2. Summary data table of results for slow cooled glass-ceramics were additives were varied and waste loading = 50 mass%, determined by XRD analysis.

Sample	Change	Phase Name	Mass%	Cell Mass	Cell Vol., Å^3	SG	*a*, Å	*c*, Å
GC-6.94-1-SC	Baseline	Oxyapatite	26.4	1694.45	549.98	P63/m	9.52	7.00
GC-6.94-1-SC	Baseline	Powellite	9.3	861.60	328.12	I41/aZ	5.30	11.68
GC-6.94-1-SC	Baseline	Cerianite	2.5	257.47	68.50	P42/nmcS	3.62	5.22
		Total crystallinity	38.2					
GC-6.94-2-SC	Low Al	Oxyapatite	22.5	1633.00	548.94	P63/m	9.52	7.00
GC-6.94-2-SC	Low Al	Powellite	9.0	861.60	321.45	I41/aZ	5.27	11.58
GC-6.94-2-SC	Low Al	Powellite2	1.1	800.06	333.33	I41/aZ	5.43	11.30
		Total crystallinity	32.6					
GC-6.94-3-SC	High B, Ca	Oxyapatite	25.5	1543.23	549.63	P63/m	9.52	7.00
GC-6.94-3-SC	High B, Ca	Powellite	9.3	861.60	326.93	I41/aZ	5.30	11.66
GC-6.94-3-SC	High B, Ca	Powellite2	0.7	800.06	335.82	I41/aZ	5.45	11.30
		Total crystallinity	35.5					
GC-6.94-4-SC	High Ca	Oxyapatite	31.1	1580.43	549.17	P63/m	9.52	7.00
GC-6.94-4-SC	High Ca	Powellite	10.9	861.60	321.72	I41/aZ	5.27	11.58
GC-6.94-4-SC	High Ca	Powellite2	1.9	800.06	332.28	I41/aZ	5.42	11.29
GC-6.94-4-SC	High Ca	Cerianite	1.0	344.22	68.44	P42/nmcS	3.62	5.22
		Total crystallinity	44.9					
GC-6.94-5-SC	High B	Oxyapatite	25.7	1608.15	550.61	P63/m	9.52	7.01
GC-6.94-5-SC	High B	Powellite	9.3	861.60	324.64	I41/aZ	5.29	11.62
GC-6.94-5-SC	High B	Powellite2	1.2	800.06	333.46	I41/aZ	5.43	11.32
GC-6.94-5-SC	High B	Cerianite	1.3	344.23	68.55	P42/nmcS	3.63	5.22
		Total crystallinity	37.5					

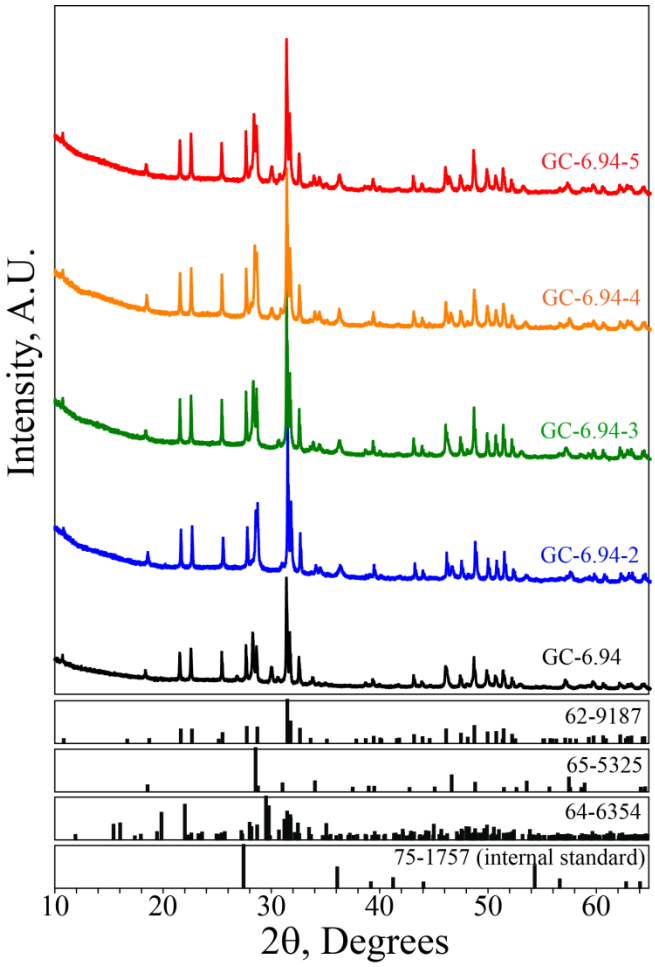

Figure 8. XRD patterns of GC-6.94 slow-cooled glass ceramics, where WL=50 mass%, and B_2O_3/alkali, CaO/MoO_3, and Al_2O_3 each varied.

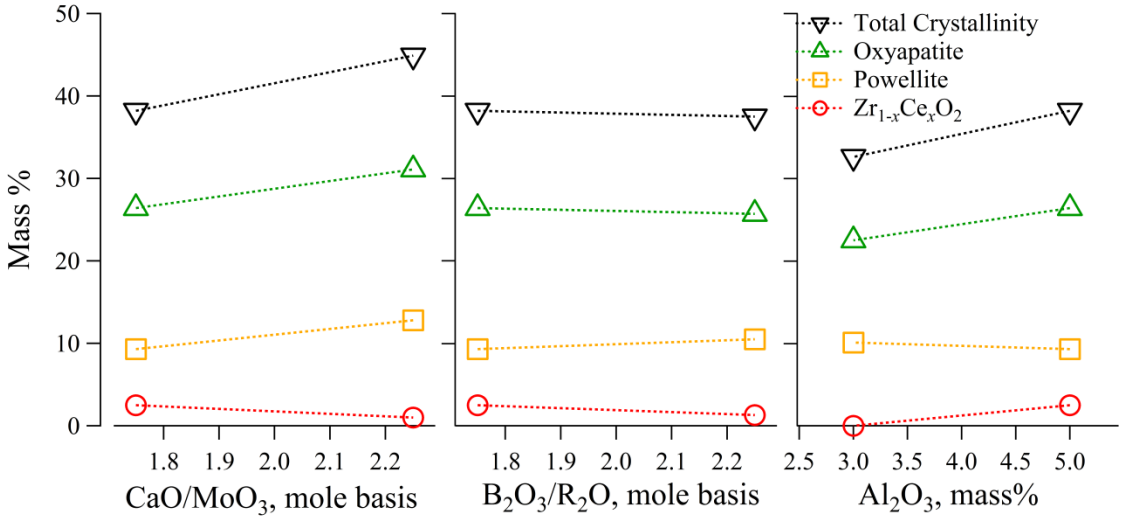

Figure 9. Crystallinity plotted as a function of one-at-a-time changes as determined by XRD.

4.2.3 X-Ray Diffraction Analysis of Isothermal Heat Treatments

Analysis of isothermal heat-treated glass ceramics by XRD was conducted to identify and quantify the crystalline phases present as a function of temperature. Figure 10 shows XRD patterns collected on GC-6.94-4 (high Ca) isothermally heat treated between 750°C and 1250°C, with SRM 674b (ZnO) spiked in as an internal standard. At 1250°C, powellite (PDF #79-2243) and ZnO (PDF# 75-0576) peaks are clearly present in the sample, and the powellite unit cell is large: a/b = 5.38 Å, c = 11.82 Å. The large unit cell at 1150°C oxyapatite (PDF# 78-1039) also appeared in the pattern and the powellite unit cell matched that seen at 1250°C. At lower temperatures, between 750 and 1050°C, the patterns all looked very similar visually. However, the powellite unit cell is noticeably smaller: a/b = 5.28 Å, c = 11.54 Å, more closely matching PDF# 85-0546, at $T \leq 1050$°C. $Zr_{1-x}Ce_xO_2$ appeared periodically as a trace phase (near detection limit) at temperatures of 850, 950, 1150, and 1250°C. The largest changes to total crystallinity occur from 1150°C–1250°C and from 1050°C–1150°C.

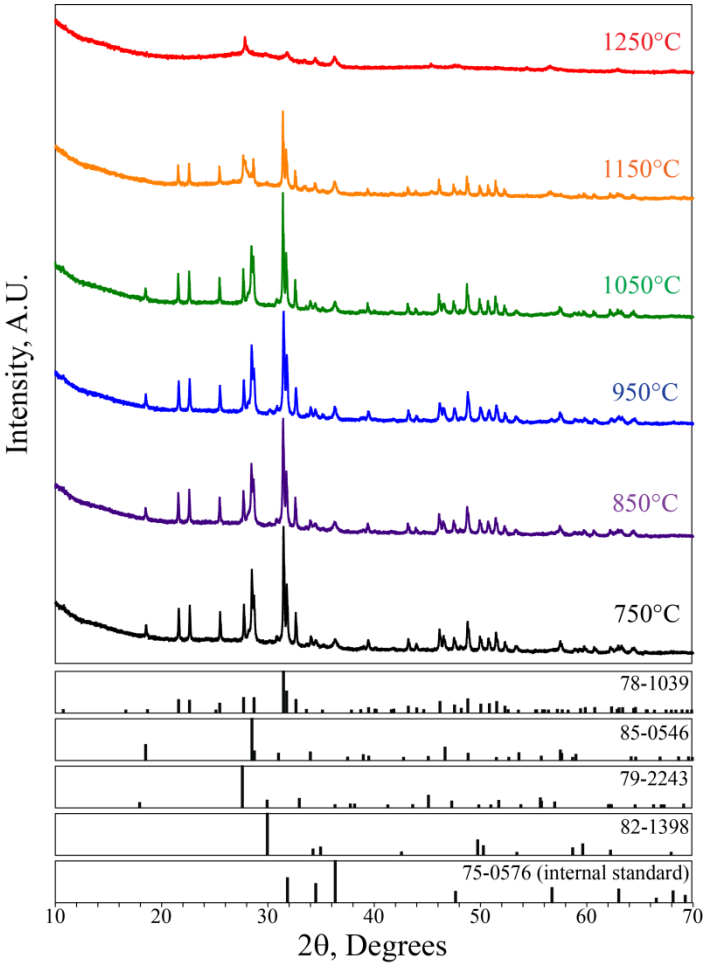

Figure 10. XRD patterns of GC-9.64-4 isothermally heat treated at 750-1250°C for 4 hours shown with identified phases and internal standards.

4.2.4 Morphology of FY 2011 Glass Ceramics

Figure 11 is a collage of SEM micrographs that show the morphology versus heat treatment conditions for the FY 2011 glass ceramics. The effect of glass additives is most pronounced in the quenched samples where $\downarrow Al_2O_3$ and $\uparrow CaO/MoO_3$ (fine scale separation) are similar but quite different from the

other two, ↑CaO +↑ B_2O_3 and ↑B_2O_3 compositions that show larger-scale separation. The 850°C, 1050°C, and slow-cooled microstructures are all similar.

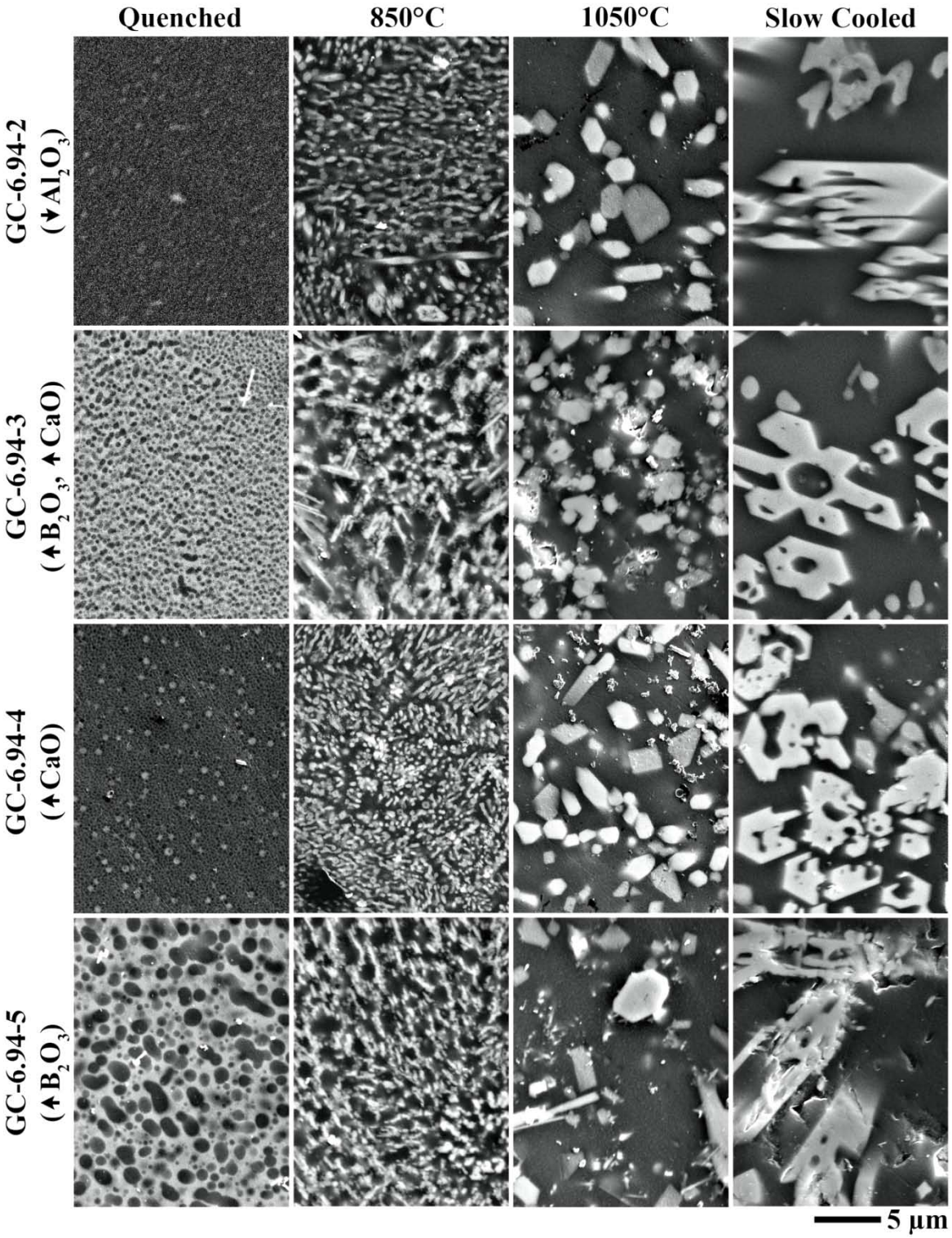

Figure 11. Secondary electron images of glass ceramics as a function of temperature history (quenched, 850°C/4hr, 1050°C/4hr, or slow cooled).

4.3 Single Phase Synthesize Results

4.3.1 Powellite

A sample of phase pure powellite ($CaMoO_4$) was successfully made at PNNL by crystallizing from a melt. A mixture of CaO and MoO_3 was heated above the melting temperature and then slowly ramped down through T_L. The sample was confirmed to be phase pure by XRD. Figure 12 shows the measured, calculated, and difference pattern obtained from whole pattern fitting process using the powellite structure. The pattern does suffer from preferred orientation, which was dealt with during Rietveld refinement of the pattern. Once preferred orientation was taken into account; the resulting difference pattern was reasonable. The unit cell parameters are in very good agreement with the literature.

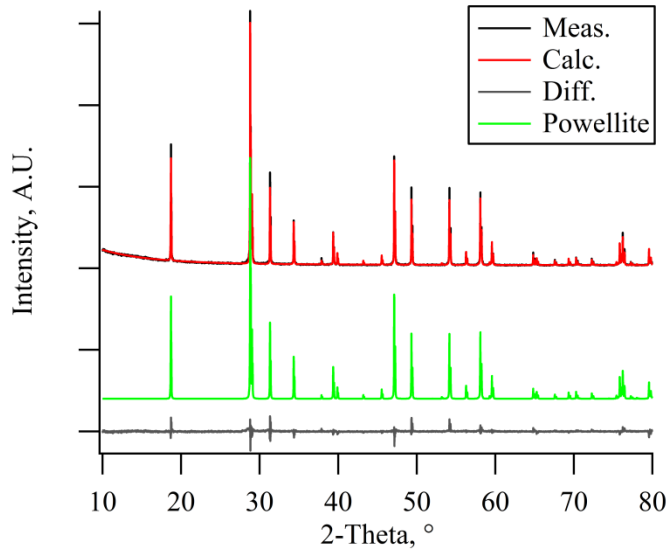

Figure 12. Rietveld refinement of powellite synthesize sample, with measured, calculated, difference, and powellite patterns.

4.3.2 Oxyapatite

A sample of phase pure oxyapatite ($Ca_2Nd_8Si_6O_{26}$) was more difficult to synthesize namely because of the high T_L near 1980°C (Bondar 1982). Preparing a sample from a mixture of oxides (ball milled) followed by traditional press and sintering was unsuccessful. XRD of the sample showed oxyapatite was the major phase; however, a significant amount of Nd_2O_3 was also observed. The results indicate the oxides were simply not mixed sufficiently to achieve a phase pure sample.

For this reason, a sol-gel process described by (Celerier et al. 2006) was followed to provide intimate mixing of the precursors. This process was followed by traditional press and sintering at a firing temperature of 1350°C. A phase-pure sample of oxyapatite was synthesized by the sol-gel process and cold press and sintering. The fitted XRD pattern shown in Figure 13 shows the measured, calculated, difference, and oxyapatite patterns determined by Rietveld refinement of the power diffraction data. The calculated pattern matches the structure well, with a very reasonable difference pattern. No additional crystalline phases were observed in the pattern. A sample was shipped to LANL for single-phase characterization studies.

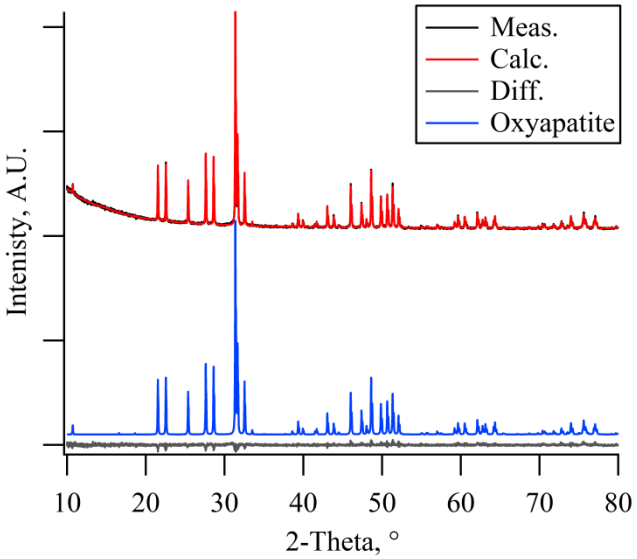

Figure 13. Rietveld refinement of oxyapatite synthesize sample, with measured, calculated, difference, and oxyapatite patterns.

4.4 Transmission Electron Microscopy/Electron Irradiation

The glass-ceramic waste form will contain several short-lived γ emitters, such as ^{137}Cs, that could lead to high dose rates and potential instability of crystalline structures in the waste form. LANL performed a series of microstructural characterization and in situ sample irradiations with 300 keV electrons generated in a Tecnai F30 TEM in the EML. By focusing electrons in the TEM on certain crystalline phases of these waste forms, it was possible to simulate radiolysis effects that might be experienced by potential glass-ceramic waste forms.

Figure 14, Figure 15, and Figure 16 show TEM/electron irradiation results on GC-6.94-SC sample. The BF image and select area electron diffraction (SAED) patterns reveal the shape and crystalline structure of different phases. EDS spectrums under STEM mode were used to decide the phase compositions. In situ electron irradiation results show that the oxyapatite and cerianite phase in the GC-6.94-SC sample exhibit stability to 1000 years at anticipated doses (2×10^{10}-2×10^{11} Gy); however, their stability may be rate dependent, which may limit the activity of the waste for which they can be employed.

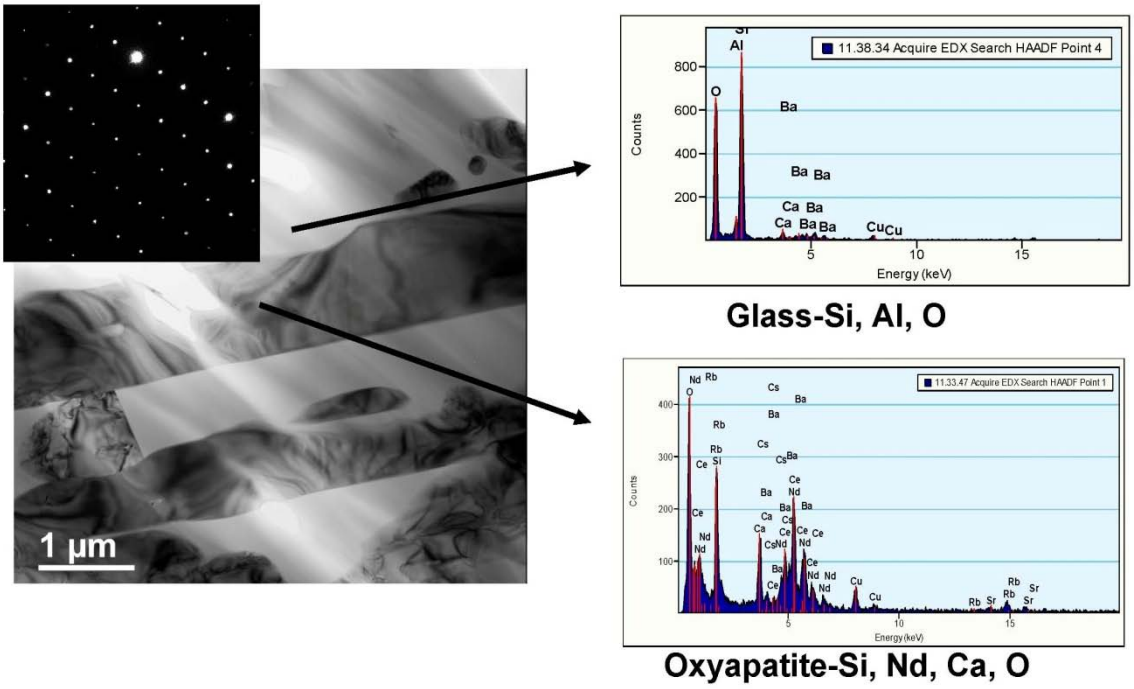

Figure 14. TEM BF image, SAED, and EDS spectrums of oxyapatite and glass phase in GC-6.94-SC sample.

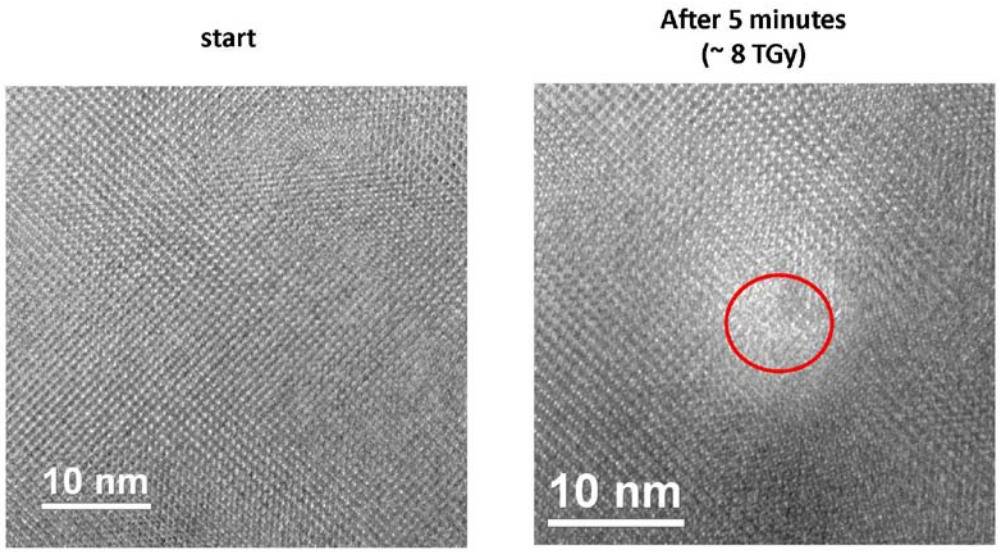

Figure 15. High-resolution TEM micrographs of GC-6.94-SC reveal that there is structural change to the crystalline structure in the oxyapatite phase, following a radiation dose at the level of 8×10^{12} Gy.

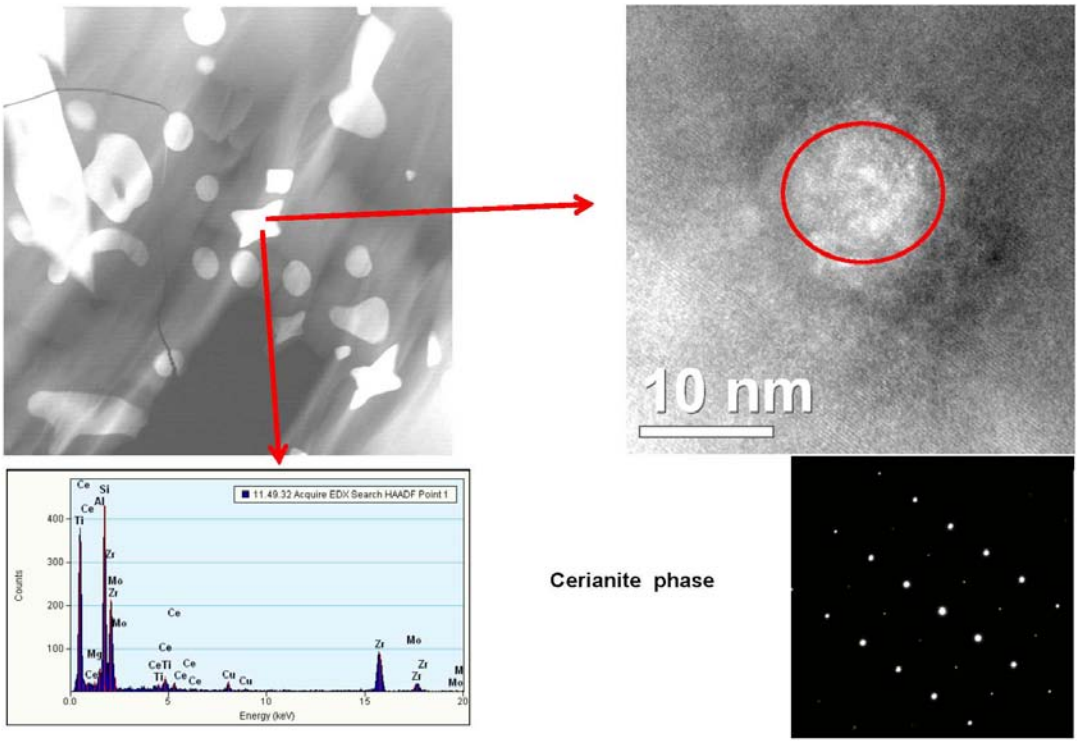

Figure 16. TEM BF image, SAED, and EDS spectrums of cerianite phase in GC-6.94-SC sample. High-resolution TEM images reveal that there is small change to the crystalline structure in the cerianite phase, following a radiation dose at the level of 8×10^{12} Gy.

Figure 17, Figure 18, and Figure 19 show TEM/electron irradiation results on the GC-5.86-SC sample. The oxyapatite phase in GC-5.86-SC (Figure 18) shows similar radiation tolerance as that in GC-6.94-SC sample (Figure 15). Interestingly, the polysome structure in RE-borosilicate phase was observed (see Figure 19). This structure is a group of crystalline compounds that possess the same types of modules in different ratios or sequences. Electron irradiation results show that an amorphization was observed in this polysome phase at a very high radiation dose level of 8 TGy (see Figure 20).

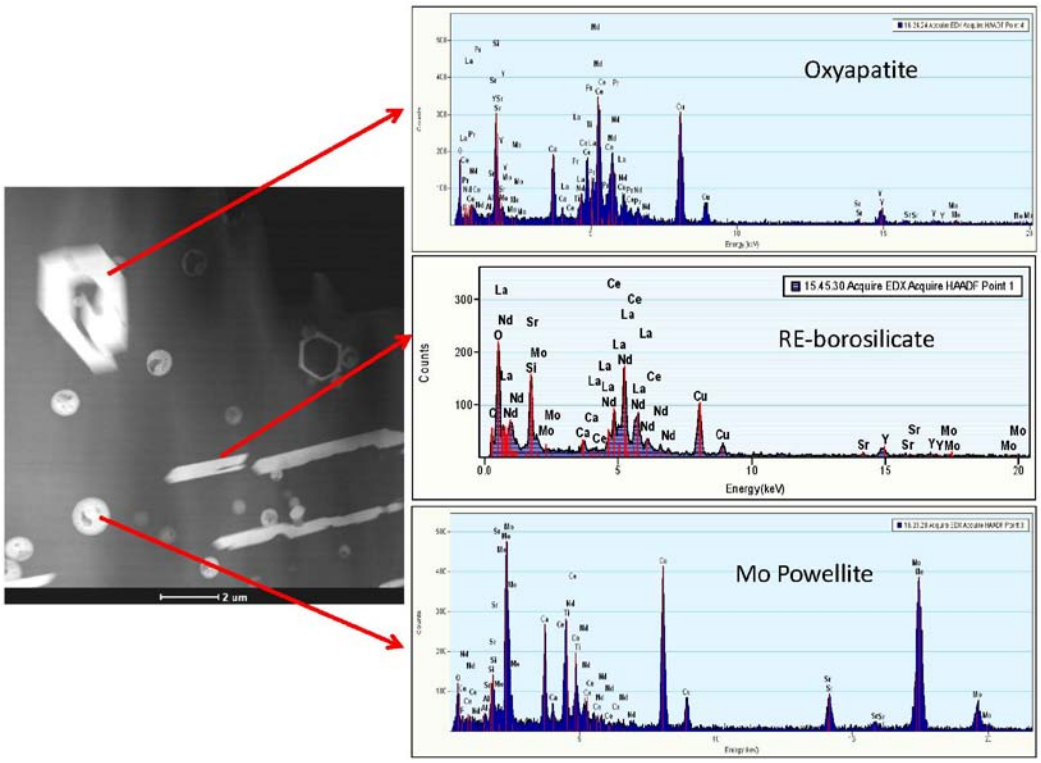

Figure 17. TEM BF image, SAED, and EDS spectrums of oxyapatite, RE-borosilicate, and Mo powellite phase in GC-5.86-SC sample.

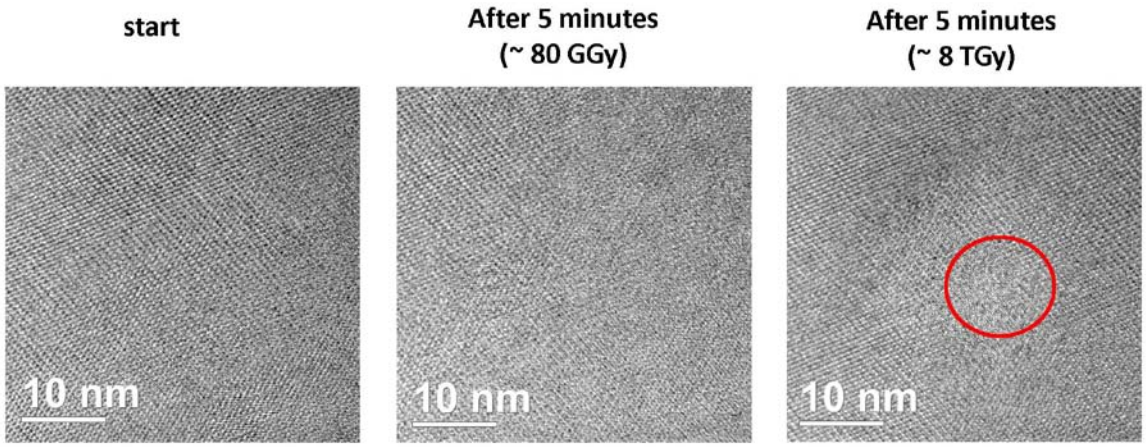

Figure 18. Microstructural evolution for the oxyapatite phase in GC-5.86-SC sample under electron irradiation at different doses.

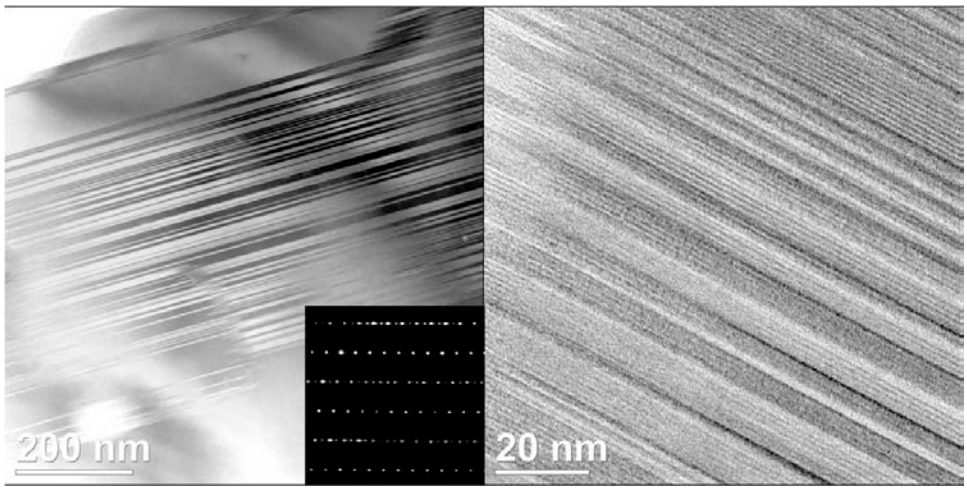

Figure 19. Polysome phenomena in RE-borosilicate phase of GC-5.86-SC sample.

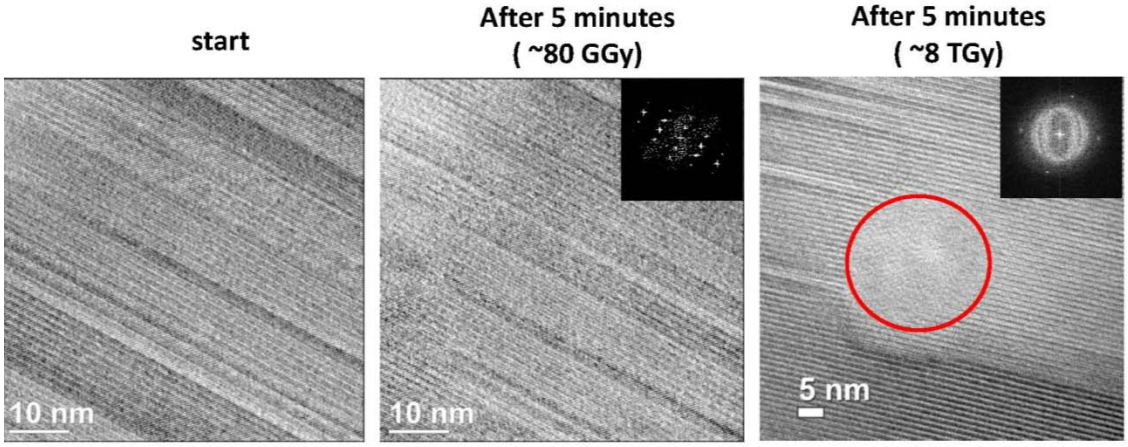

Figure 20. High-resolution TEM images and Fast Fourier transform reveal there is amorphization in the RE-borosilicate phase of GC-5.86-SC sample, following a radiation dose at the level of 8×10^{12} Gy.

Figure 21 and Figure 22 show the electron irradiation study for single-phase powellite $CaMoO_4$ samples that were synthesized at PNNL (see Section 4.3.1). The results suggest this powellite phase exhibits stability to 1000 years at anticipated doses (2×10^{10}-2×10^{11} Gy) but becomes amorphous at higher doses between 10^{12} and 10^{13} Gy. The radiation tolerance of $CaMoO_4$ samples from PNNL were similar to $CaMoO_4$ samples fabricated by the Savannah River National Laboratory.

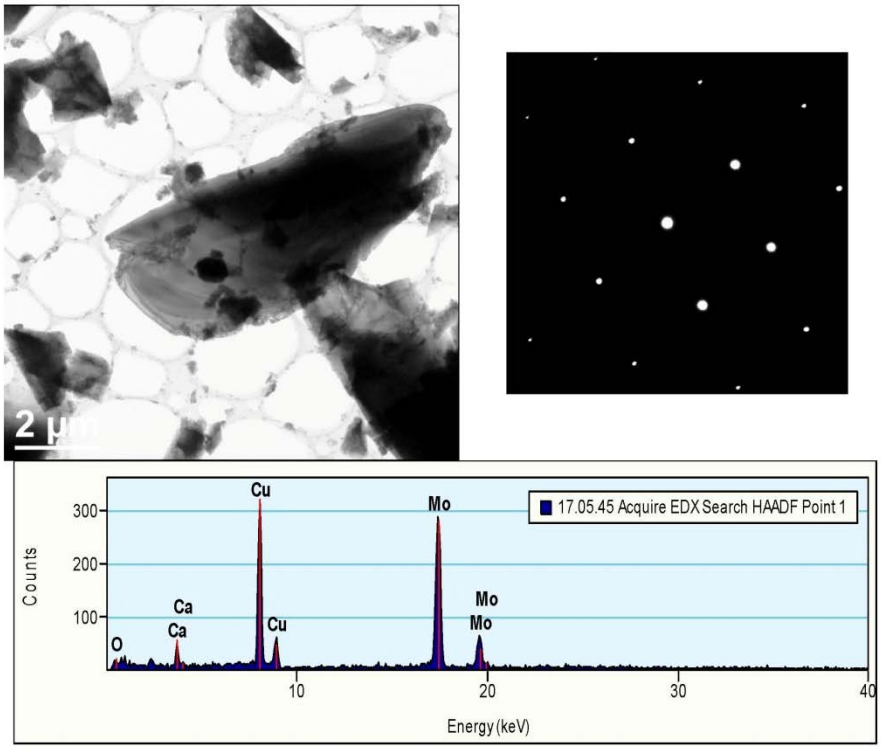

Figure 21. TEM BF image, SAED, and EDS spectrums of single phase $CaMoO_4$ powellite sample.

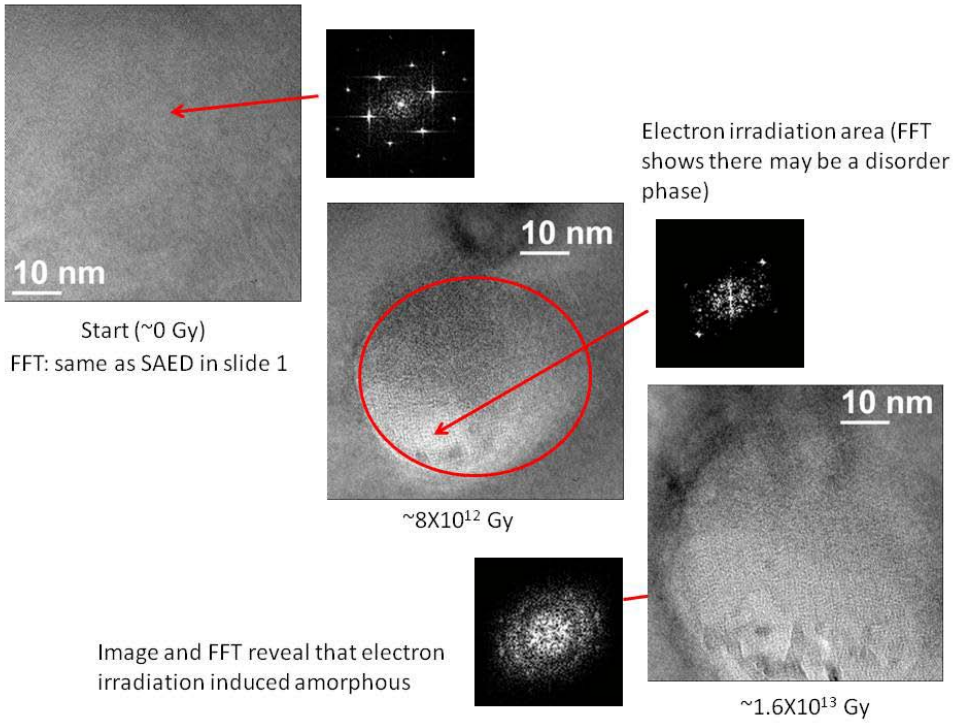

Figure 22. Microstructural evolution for phase-pure $CaMoO_4$ sample under electron irradiation at different doses.

The stability ranges measured in situ with TEM are adequate for the short-lived isotopes in the combined CS + Ln + TM waste stream. The calculated cumulative dose is ~7×10^{9} Gy, which is below the stability range measured by TEM at 2×10^{10}–2×10^{11} Gy, shown in Figure 23. The maximum dose in the waste form will be achieved in ~100 years, again due to the short-lived isotopes in the waste. These calculations are based on a glass ceramic, at waste load 50 mass%, and a fuel with a burnup of 51 GWd/metric tons of initial heavy metal (MTIHM) cooled for 5 years before treatment.

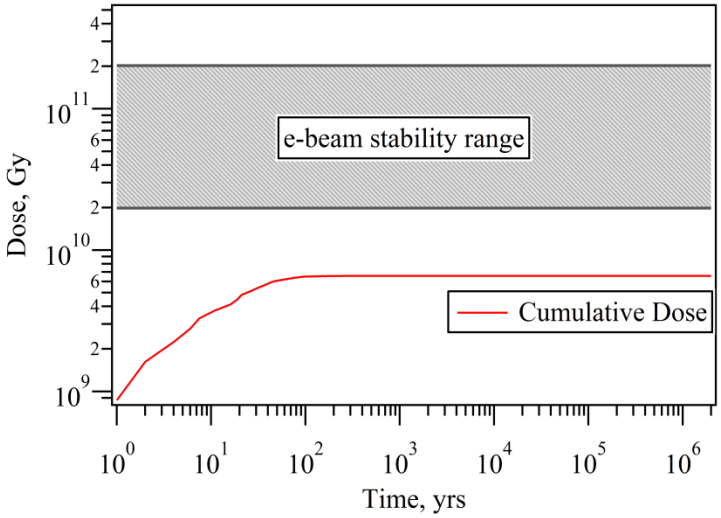

Figure 23. Cumulative dose versus time for glass ceramic at 50 mass% waste load, 51 GWd/MTIHM fuel cooled 5 years prior to immobilization.

4.5 Ion Beam Irradiation

4.5.1 Ion Irradiation of Complex Glass Ceramics Fabricated at Pacific Northwest National Laboratory

Glass ceramics with molybdenum content of 6.94% (GC-6.94-SC) and 5.86% (GC-5.86-SC), which were synthesized by PNNL, were irradiated at room temperature. Alpha particles (5 MeV) were used to simulate self-radiation effects in a waste form. Based on the stopping and range of ions in matter simulations in silica, the peak radiation dose in these experiments was 1.9 GGy for GC-5.86-SC and 2.4 GGy for GC-6.94-SC.

Because samples have a strong preferred orientation, the XRD measurements on pristine and irradiated samples were made with rotation of at least one revolution per step to minimize effects of sample positioning. XRD characterizations (Figure 24 and Figure 25) revealed there were no changes in both samples if compared before and after irradiations. The results match with data results for 3 MeV proton irradiation test on GC-6.94-SC conducted in FY 2010.

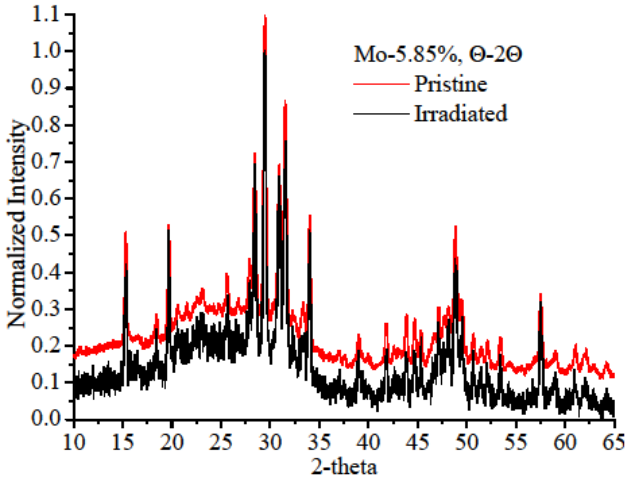

Figure 24. XRD results on GC-5.86-SC sample before and after α-irradiation.

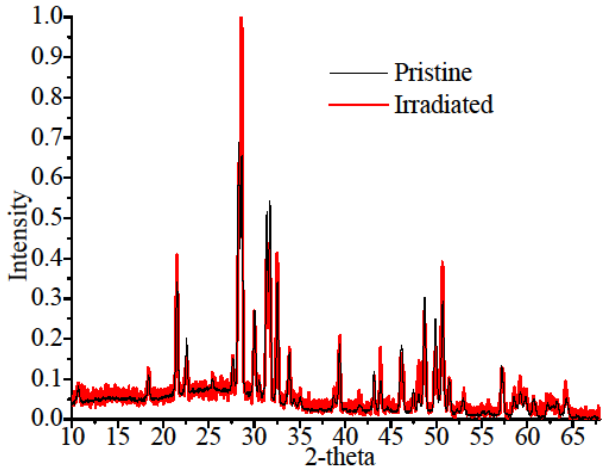

Figure 25. XRD results on GC-6.94-SC sample before and after α-irradiation.

4.5.2 Preparation and Ion Irradiation of Model Single-Phase Glass Ceramic Fabricated at Los Alamos National Laboratory

Table 3 summarizes experiments on synthesis of model Nd-Mo and oxyapatite glass ceramics. During experiments on oxyapatite, it was discovered that with 1200°C as maximum temperature, compositions should be limited to high alkali content (experiments # 4, 5 given in Table 3) to achieve melting and homogenization. Nd-Mo model glass ceramics were irradiated with 5 MeV He and extensively characterized before and after irradiation.

Table 3. Summary of experiments on synthesis of model glass ceramics.

#	Composition, mole%					Heat-Treatment	Phase Composition	Notes
	Nd_2O_3	SiO_2	B_2O_3	CaO	Na_2O			
1	5.5	71.5	11.0	1.4	10.6	1150°C, cooled at10°C/min	Nd-silicate, Na/Nd-oxyapatite, cristobalite, glass	Glass with embedded crystals.
2	4.3	75.6	10.5	4.3	5.2	1150°C, 1200°C, quenched to RT	Na/Nd-oxide, Nd-oxide, tridimite (HT SiO_2), Nd-silicate, $Ca_3B_4(OH)_{16}$	Decrease in Na content revealed that with thermal treatment capabilities (≤ 1200°C), the mixture cannot be melted. Heat treatment resulted in coarsened agglomerates of crystals.
3	4.3	75.6	10.5	4.3	5.2	1150°C, 1200°C, quenched to RT	Na/Nd-oxide, Nd-oxide, tridimite (HT SiO_2), Nd-silicate, $Ca_3B_4(OH)_{16}$	Repeated two times with thorough grinding and same result.
4	5.2	68.4	10.5	5.2	10.6	1150°C, 1200°C, quenched to RT	Amorphous glass with small amount of Na/Nd-oxyapatite	Translucent sample; no signs of crystallization.
5	5.2	68.4	10.5	5.2	10.6	Quenched glass was heated to 1200°C, quenched to 700°C, held for 3 hrs, and then cooled to RT at 1°C/min	XRD spectra not measured because of long-term instrument problems	Translucent sample; no signs of crystallization.

RT: Room temperature

HT: High temperature

Analysis of Nd/Mo borosilicate glass ceramics provided data on microstructure, phase composition, and response to 5 MeV He^+ irradiations at room temperature. STEM samples of slowly cooled and quenched glass ceramics were prepared to improve spatial resolution of EDS mapping because microstructural features of interest were < 200 nm. To eliminate strong charging, STEM samples were coated from both sides by a 2-nm layer of carbon. Polished monolithic samples of pristine and irradiated quenched glass ceramics were also coated by a 2-nm carbon layer before SEM measurements. Improved (better signal-to-noise) composition maps for slowly cooled sample were acquired.

SEM observations showed that as-quenched glass ceramics consist of crystalline islands of ~80 and ~500 nm. Upon cooling, the size of islands increases to ~3 um and 500 nm and two-liquid phase separation occurs in the glass phase.

Compositional mapping (Figure 26) confirmed that big precipitates after both types of thermal treatments include Na, Nd, Mo, and O. This is consistent with XRD that both samples consist of $Na_{0.5}Nd_{0.5}Mo^{6+}O_4$ and $Na_2Mo^{6+}{}_2O_7$. X-ray absorption near edge structure (XANES) analysis on a pristine quenched sample and X-ray photoelectron spectroscopy (XPS) measurements on an in-situ cleaved cooled sample confirmed the phase composition and showed that all Mo in both samples has a 6+ coordination number. Compositional mapping also revealed that two-liquid phase separation upon cooling is caused by Na redistribution.

XRD was measured on a polished monolith in θ-2θ and grazing incidence modes with parallel beam before and after irradiations. XRD measurements did not indicate changes after irradiations, as shown in Figure 27. The sample was irradiated to an ionizing dose of 2.5–5.5 GGy as calculated from the stopping and range of ions in matter simulation (Figure 28).

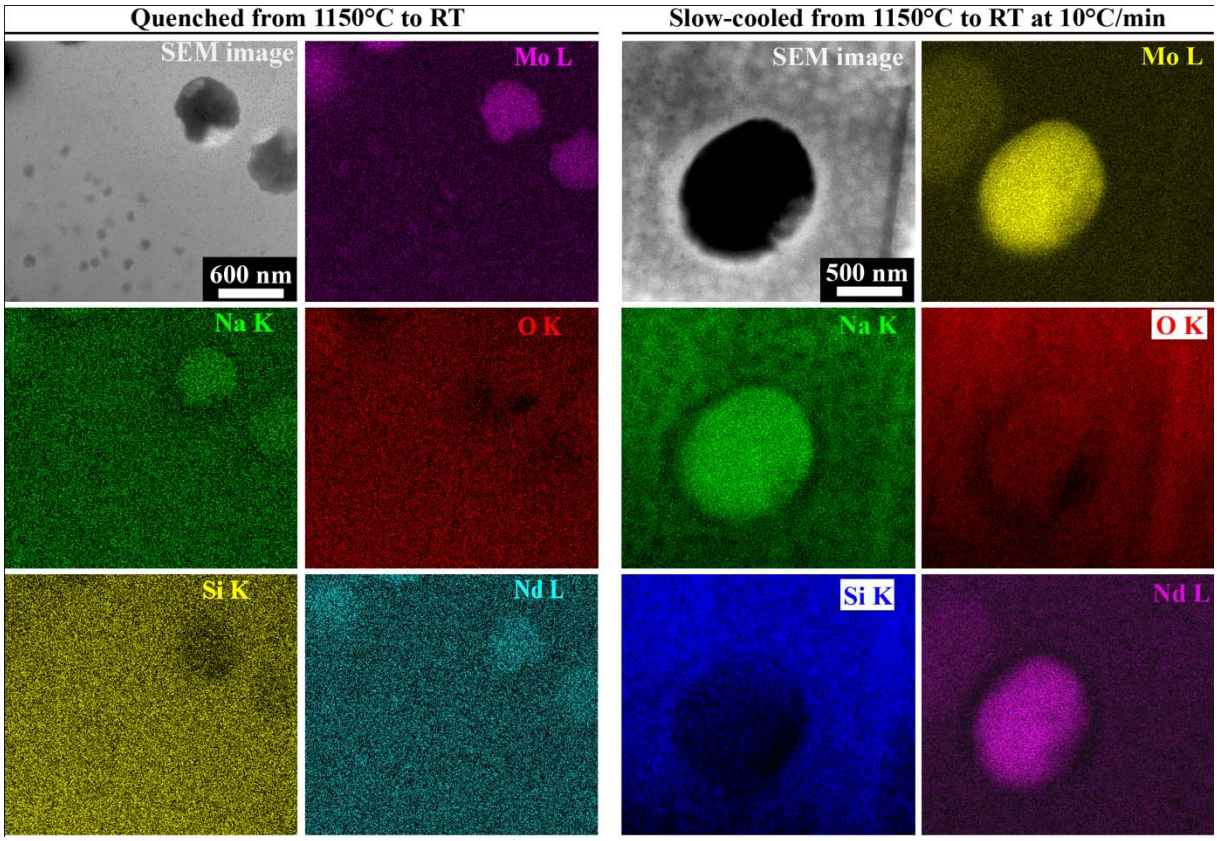

Figure 26. STEM/SEM compositional analysis of quenched and cooled Nd-Mo glass ceramics.

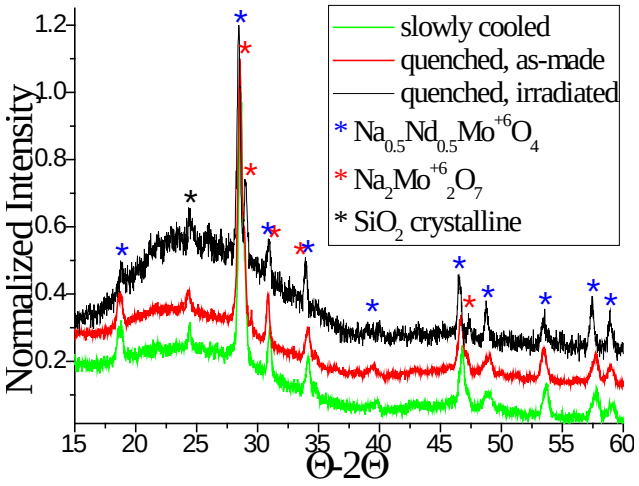

Figure 27. XRD profiles of quenched and cooled Nd-Mo glass ceramics.

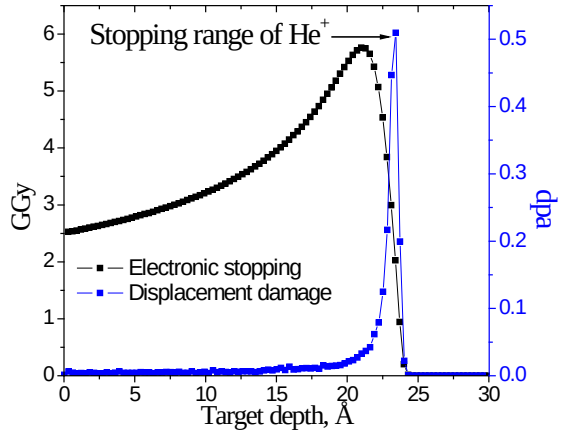

Figure 28. Ionization and damage profile for 5 MeV He in Nd-Mo glass ceramics.

A significant change in color was observed in the irradiated sample. The color was similar to one that appeared as a result of surface sputtering with 4 eV Ar^+ before XPS measurements (Figure 29). After sputtering procedure in these conditions, Mo on the sample surface appeared to be reduced. Sputtering at mild conditions (1 eV Ar^+) did not result in Mo reduction. To realize whether color change is caused by bulk or surface effect XANES and extended X-ray absorption fine structure spectroscopy (EXAFS) measurements were conducted. X-ray penetration depth is high (could be tenths of microns depending on material's composition and density), however it is comparable with depth of damaged layer caused by He^+ ions. Therefore the measurements were done in fluorescence mode.

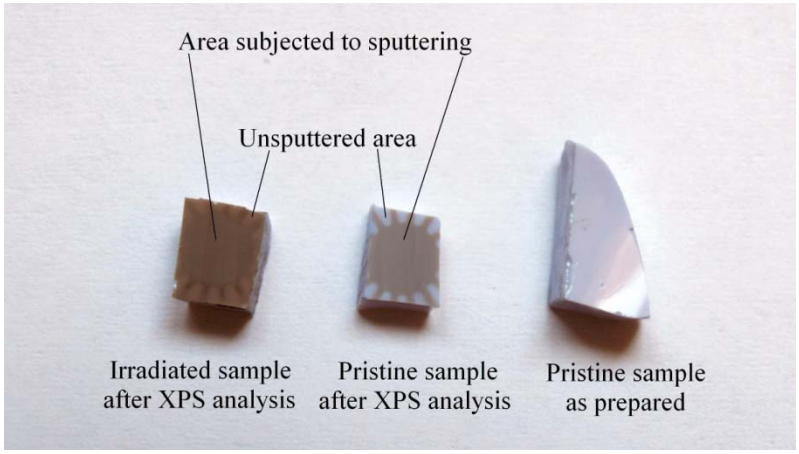

Figure 29. View of samples before and after XPS

Neither XANES nor EXAFS measurements conducted on pristine and irradiated quenched samples revealed any reduction of Mo or changes in local environment as a result of irradiation. The stopping and range of ions in matter simulation of sputtering indicated that oxygen is primarily sputtered out and thus causes Mo reduction at the surface. Back-scattered SEM micrographs (Figure 30) revealed that although no changes occurred in crystalline phase after irradiation as detected by spectroscopy and XRD, there is increased precipitation around big islands. Note that pristine and irradiated samples were taken from the same location as the as-prepared sample. The effect should be more pronounced after similar irradiation is made at high temperature (300–400^{o}C).

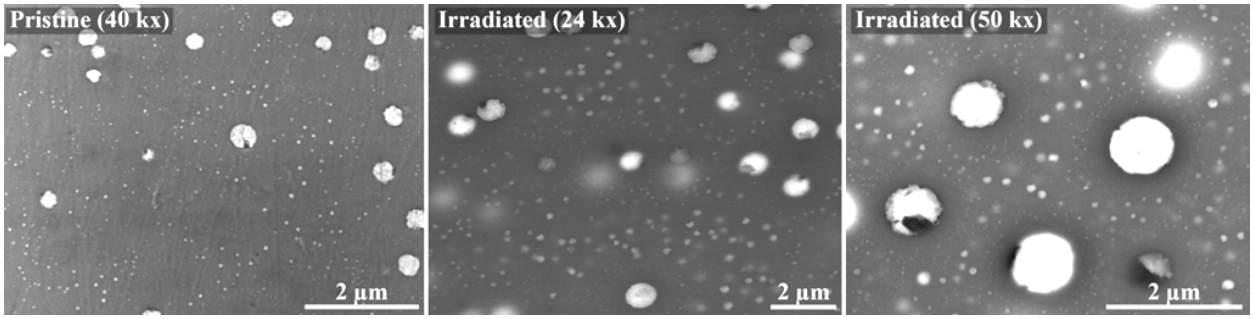

Figure 30. SEM micrographs of pristine and irradiated Nd-Mo glass ceramics.

4.6 Mechanical Properties Test on GC-4 (FY 2010 Option 1) Samples Before and After Ion Irradiation Using Nano-Indentation Technique

Nano-indentation experiments were performed on certain crystalline phases of GC-4 samples before and after alpha irradiation at a dose of 8 GGy to determine the effects of ion irradiation on mechanical properties. Figure 31 shows the schematic draw of nano-indentation experiments and nano-indents in the SEM image. The Young's modulus and the hardness of Ln-borosilicate and oxyapatite phases in GC-4 samples shows there are subtle changes before and after ion irradiation (Figure 32). This result suggests mechanical property of these crystalline phases is very stable under irradiation.

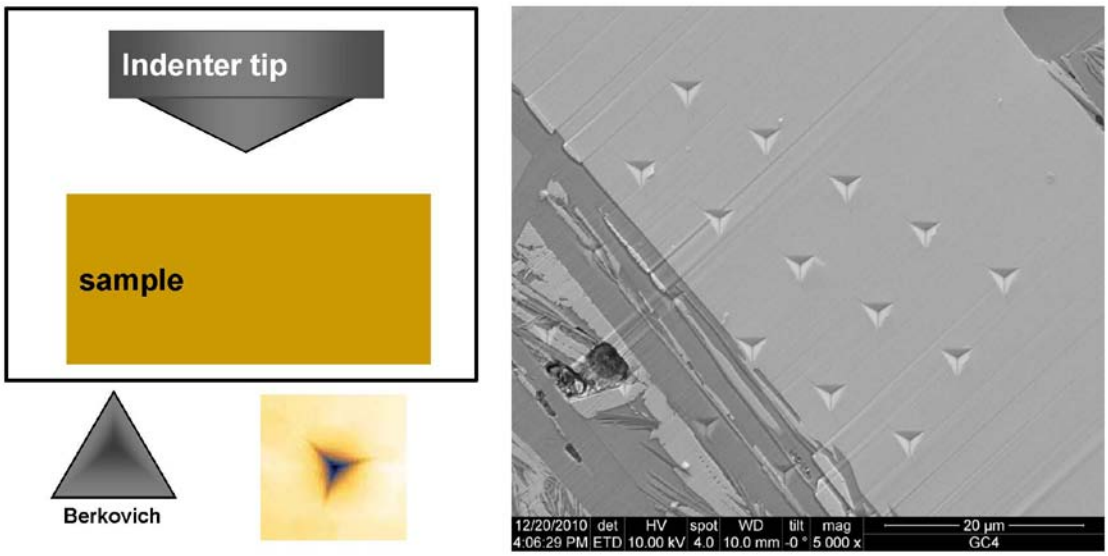

Figure 31. Schematic draw of nano-indentation experiments.

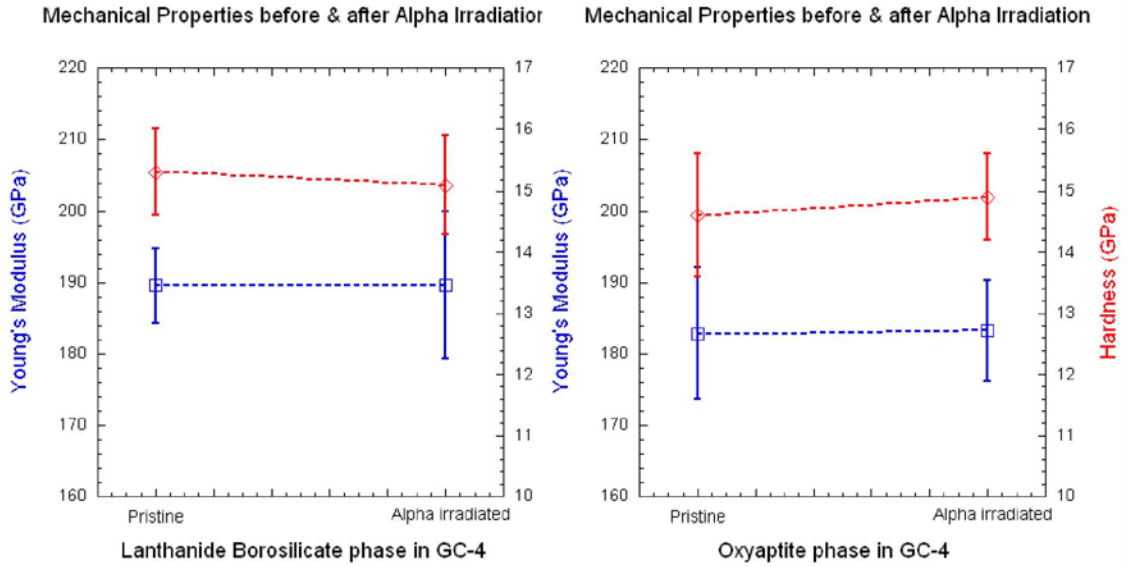

Figure 32. Nano-indentation measurements of Young's modulus (left), and the hardness (right) on different crystalline phases.

5. CONCLUSIONS

Silicate based glass-ceramic waste form continues to show promise for immobilization of combined CS + TM + Ln fission products waste streams (Option 2). The static leach testing results, for durations up to 28 days, show normalized concentrations on par with durable waste glasses such as the LRM glass, according to the PCT-B.

New glass-ceramic compositions provide better understanding of the effect of Al_2O_3, CaO/MoO_3 and B_2O_3/alkali molar ratios on the microstructure and stability of phases formed when quenched from a melt, and as a function of temperature and cooling history. Similar crystalline phases were observed in all of the slow-cooled glass ceramics, showing some flexibility in terms of composition while maintaining the

targeted phases. Synthesis of phase-pure powellite and oxyapatite were each successful and provide an opportunity to study both the leach rate and irradiation stability without interactions of the multi-phase glass ceramics. The irradiation stability of powellite was measured with the single-phase sample, which would be difficult to measure in the multi-phase glass ceramic waste forms because of the small heterogeneous powellite inclusions. Ion irradiation and in situ TEM observations indicate these crystalline phases (e.g., oxyapatite, powellite, and Ln-borosilicate) in silicate-based glass ceramic waste forms exhibit stability to 1000 years at anticipated doses (2×10^{10}-2×10^{11} Gy), which appear adequate for the short-lived isotopes resulting in calculated cumulative dose of ~7×10^{9} Gy over 100 years (at 50 mass% waste load) after which additional dose is negligible.

6. FUTURE WORK

The following tasks are planned for FY 2012:

1. A glass ceramic composition will be selected and fully characterized in support of an induction cold crucible melter test
2. A matrix of glass ceramics will vary key waste components (MoO_3, ZrO_2, and Ln_2O_3), along with further variations of additives (CaO, B_2O_3, Al_2O_3, and SiO_2)
3. High-spatial resolution characterization will be done with TEM; electron and ion irradiation experiments will be used to simulate self-irradiation and test the stability and durability of glass ceramic waste forms, including irradiations at different temperatures and dual-beam ion irradiations
4. Thermophysical property measurement capability will be used to test thermal properties (including thermal conductivity, thermal diffusivity, and specific heat capacity)
5. Mechanical properties measurements (including fracture toughness, Young's modulus, and hardness) of glass ceramics will be tested.

7. REFERENCES

André, L. 2004. *RPP Pilot Melter Prototypic LAW and HLW Canister Glass Fill Test Results Report*. Report No. TRR-PLT-080, Duratek Inc, Columbia, Maryland.

Bondar, IA. 1982. "Rare-Earth Silicates." *Ceramics International* 8(3):83-89.

Caurant, D, O Majerus, E Fadel, and M Lenoir. 2007. "Effect of Molybdenum on the Structure and on the Crystallization of SiO_2–Na_2O–CaO–B_2O_3 Glasses." *J. Am. Ceram. Soc.* 90(3):774-83.

Celerier, S, C Laberty, F Ansart, P Lenormand, and P Stevens. 2006. "New Chemical Route Based on Sol Gel for the Synthesis of Oxyapatite $La_{9.33}Si_6O_{26}$." *Ceramics International* 32(3):271-76.

Cheary, RW, AA Coelho, and JP Cline. 2004. "Fundamental Parameters Line Profile Fitting in Laboratory Diffractometers." *J. Res. Natl. Inst. Stand. Technol.* 109:1-25.

Crum, JV, AL Billings, J Lang, JC Marra, C Rodriguez, JV Ryan, and JD Vienna. 2009. *Baseline Glass Development for Combined Fission Products Waste Streams*. Report No. AFCI-WAST-WAST-MI-DV-2009-000075, Pacific Northwest National Laboratory, Richland, Washington.

Crum, JV, LR Turo, BJ Riley, M Tang, A Kossoy, and KE Sickafus. 2010. *Glass Ceramic Waste Forms for Combined CS+LN+TM Fission Products Waste Streams*. Report No. FCRD-WAST-2010-000181, Pacific Northwest National Lab, Richland, Washington.

Ebert, WL, and VN Zyryanov. 2000. "Round-Robin Testing of a Standard Material for Acceptance Testing of Low-Activity Radioactive Waste Products." *Ceramic Transactions* 107:409-16.

Glass Batching and Melting. Report No. Technical Procedure GDL-GBM, Rev. 3., Pacific Northwest National Laboratory, Richland, WA.

Gombert, I, D., C D., J., W Ebert, S Piet, T Trickel, and J Vienna, eds. 2009. *"A Trade Study for Waste Concepts to Minimize HLW Volume"*. Materials Research Society, Pittsburg, Pennsylvania.

Petkus, LL. 2003. *Canister Centerline Cooling Data, Rev. 1*. Report No. RPP-WTP Memorandum, R10152486, Waste Treatment Plant, Richland, Washington.

Ryan, JV, EC Buck, J Chun, JV Crum, BJ Riley, DM Strachan, SK Sundaram, LA Turo, and JV Vienna. 2009. *Alternate Waste Forms: Aqueous Processing*. Report No. AFCI-WAST-PMO-MI-DV-2009-000360, Pacific Northwest National Laboratory, Richland, Washington.

ASTM C-1285-02, "Standard Test Methods for Determining Chemical Durability of Nuclear, Hazardous, and Mixed Waste Glasses and Multiphase Glass Ceramics: The Product Consistency Test (PCT)," ASTM International, West Conshohocken, Pennsylvania, 2002.

SRM 674b, "X-ray Power Diffraction Intensity Set for Quantitative Analysis by X-Ray Diffraction," National Institute of Standards and Technology, Department of Commerce, Gaithersburg, Maryland, 2007.